UNIVERSIDADE ESTADUAL DE CAMPINAS
Faculdade de Engenharia Mecânica

Andrea Carolina Corredor Bedoya

Acoustic characterization of mortar and tire rubber composites for noise insulation

Caracterização acústica de compósitos de argamassa e borracha de pneus para isolamento de ruído

CAMPINAS
2016

Andrea Carolina Corredor Bedoya

Acoustic characterization of mortar and tire rubber composites for noise insulation

Caracterização acústica de compósitos de argamassa e borracha de pneus para isolamento de ruído

Master Thesis presented to the school of Mechanical Engineering of the University of Campinas in partial fulfillment of the requirements for the degree of Master in Mechanical Engineering, in the Area of Solid Mechanics and Mechanical Design.

Dissertação de Mestrado apresentada à Faculdade de Engenharia Mecânica da Universidade Estadual de Campinas como parte dos requisitos exigidos para a obtenção do título de Mestra em Engenharia Mecânica, na Área de Mecânica dos Sólidos e Projeto Mecânico.

Orientador: Prof. Dr. Alberto Luiz Serpa

ESTE EXEMPLAR CORRESPONDE À VERSÃO FINAL DA TESE DEFENDIDA PELA ALUNA ANDREA CAROLINA CORREDOR BEDOYA, E ORIENTADA PELO PROF. DR. ALBERTO LUIZ SERPA

Alberto Luiz Serpa.
ASSINATURA DO ORIENTADOR

CAMPINAS
2016

Agência(s) de fomento e nº(s) de processo(s): CAPES, 33003017

Ficha catalográfica
Universidade Estadual de Campinas
Biblioteca da Área de Engenharia e Arquitetura
Elizangela Aparecida dos Santos Souza - CRB 8/8098

C824a
Corredor Bedoya, Andrea Carolina, 1990-
Acoustic characterization of mortar and tire rubber composites for noise insulation / Andrea Carolina Corredor Bedoya. – Campinas, SP : [s.n.], 2016.

Orientador: Alberto Luiz Serpa.
Dissertação (mestrado) – Universidade Estadual de Campinas, Faculdade de Engenharia Mecânica.

1. Absorção do som. 2. Isolamento acústico. 3. Argamassa. 4. Pneus - Reaproveitamento. 5. Compósito. I. Serpa, Alberto Luiz,1967-. II. Universidade Estadual de Campinas. Faculdade de Engenharia Mecânica. III. Título.

Informações para Biblioteca Digital

Título em outro idioma: Caracterização acústica de compósitos de argamassa e borracha de pneus para isolamento de ruído
Palavras-chave em inglês:
Sound absorption
Soundproofing
Mortar
Tires - Reuse
Composite
Área de concentração: Mecânica dos Sólidos e Projeto Mecânico
Titulação: Mestra em Engenharia Mecânica
Banca examinadora:
Alberto Luiz Serpa [Orientador]
José Roberto de França Arruda
Stelamaris Rolla Bertoli
Data de defesa: 19-05-2016
Programa de Pós-Graduação: Engenharia Mecânica

UNIVERSIDADE ESTADUAL DE CAMPINAS
FACULDADE DE ENGENHARIA MECÂNICA
COMISSÃO DE PÓS-GRADUAÇÃO EM ENGENHARIA MECÂNICA
DEPARTAMENTO DE MECÂNICA COMPUTACIONAL

DISSERTAÇÃO DE MESTRADO ACADÊMICO

Acoustic characterization of mortar and tire rubber composites for noise insulation

Caracterização acústica de compósitos de argamassa e borracha de pneus para isolamento de ruído

Autor: Andrea Carolina Corredor Bedoya
Orientador: Prof. Dr. Alberto Luiz Serpa

A Banca Examinadora composta pelos membros abaixo aprovou esta Dissertação:

Alberto Luiz Serpa.

Prof. Dr. Alberto Luiz Serpa
DMC/FEM/UNICAMP

Prof. Dr. José Roberto de França Arruda
DMC/FEM/UNICAMP

Profa. Dra. Stelamaris Rolla Bertoli
DAC/FEC/UNICAMP

Campinas, 19 de Maio de 2016.

Dedico este trabajo a mi familia, mis papás y mi hermana, por apoyarme siempre.

Acknowledgments

A mi papá Fabio Corredor por sus consejos personales y profesionales.

A mi mamá Consuelo Bedoya por apoyarme siempre.

A mi hermana Laura Corredor por siempre escucharme y ayudarme.

Ao meu orientador, Prof. Dr. Alberto Luiz Serpa, pela orientação, ajuda e confiança.

À Rita Aparecida Zoppi, pela ajuda no desenvolvimento deste trabalho e na caracterização do pó de borracha incluída no Anexo A deste trabalho.

A todos os meus colegas de sala, Ana, Fuga, Amanda, Ruth, Richard, Ramiro, Luis, Carlos e Camilo pela ajuda tanto pessoal quanto acadêmica.

Às meninas que foram minha família Brasileira, Thaís, Amanda, Lígia, Gabriela e Mariana.

A todos os meus amigos que fizeram parte deste processo de aprendizado.

À Profa. Dra. Maria do Carmo Gonçalves do Instituto de Química da UNICAMP e à Profa. Dra. Eliana Aparecida de Rezende Duek da Pontifícia Universidade Católica de São Paulo pelo apoio na utilização dos equipamentos necessários para a caracterização do pó de borracha.

Ao Prof. Dr. Marcos Akira d'Avila pela disponibilização do Laboratório de Biopolímeros e Eletrofiação;

Aos senhores Haroldo Luis de Oliveira e Paulo Laureano Garcia pela apoio na preparação dos suportes de concreto para os ensaios de aderência.

Ao pessoal do LNNano pela ajuda durante os experimentos realizados.

Ao pessoal do LabEDin pela disposição e orientação nos experimentos.

À Borcol Tapetes Automotivos pela doação do pó de borracha para a execução deste projeto, e à Pirelli Pneus pela doação da borracha de estireno-butadieno.

À Faculdade de Engenharia Mecânica da UNICAMP pela oportunidade de realizar este trabalho.

À Coordenação de Aperfeiçoamento de Pessoal de Nível Superior (CAPES) pelo apoio financeiro.

A todas as pessoas que contribuíram direta ou indiretamente para o desenvolvimento deste trabalho.

Resumo

Corredor-Bedoya, A.C. Caracterização acústica de compósitos de argamassa e borracha de pneus para isolamento de ruído. 2016. 96p. Tese (Mestrado). Faculdade de Engenharia Mecânica, Universidade Estadual de Campinas - UNICAMP, Campinas.

Pneus de automóveis são descartados gerando sérios problemas ao meio ambiente devido ao tempo de decomposição da borracha. Uma alternativa para minimizar esse problema é triturar os pneus para serem usados como agregados em materiais compósitos, principalmente no campo da construção civil. Este trabalho apresenta o estudo do comportamento acústico de compósitos de argamassa colante e pó de borracha de pneus inservíveis. Foram preparados compósitos contendo 10, 15 e 25% em massa de pó de borracha, cuja granulometria foi de 18 a 35 mesh, e de 35 a 60 mesh. Foram analisados o coeficiente de absorção e a perda de transmissão sonora, visando a minimização da transmissão de som através de um sistema de piso. Foram realizados alguns pré-testes, obtendo três níveis de partículas de borracha na mistura da argamassa e duas granulometrias das partículas de borracha para o preparo das amostras. O experimento foi feito usando um tubo de impedância usando-se o *Método de Um Microfone* para ambas configurações e o método de uma carga na medição da perda de transmissão para a faixa de frequência de 400 Hz a 2500 Hz. Uma simulação de um sistema de piso de três camadas foi feita, incluindo a argamassa pura e as amostras preparadas para estudar o comportamento do conjunto. Os resultados apresentaram uma forte relação entre o coeficiente de absorção e a composição para as duas granulometrias: quanto maior a quantidade de partículas de borracha na argamassa, maior o coeficiente de absorção. Para a perda de transmissão, os resultados parecem estar mais influenciados pela granulometria do que pela composição, verificando-se que para amostras com partículas de borracha maiores, existe uma melhora no isolamento acústico, tanto na análise experimental dos compósitos, quanto na simulação do sistema de piso. O comportamento mecânico dos compósitos também foi estudado, testando-se a resistência de aderência à tração dos compósitos fabricados e comparando os resultados com a resistência da amostra de argamassa pura. Os resultados mostraram uma diminuição na resistência de aderência dos compósitos testados.

Palavras-chave: Coeficiente de absorção, perda de transmissão, argamassa colante, partículas de borracha de pneus descartados, compósito.

Abstract

Corredor-Bedoya, A.C. Acoustic characterization of mortar and tire rubber composites for noise insulation. 2016. 96p. Master thesis. School of Mechanical Engineering, University of Campinas, Campinas.

Automotive tires are discarded causing an environmental problem due to the time they take to decompose completely. One alternative is to crush them in order to use them as an aggregate for composites materials, mainly in the construction field. This work presents the study of the acoustic behavior of samples made of adhesive mortar and scrapped tire rubber particles, with different mortar/rubber proportions and rubber particle size. The interest is to study the combination of mortar/rubber proportion and rubber particle size through the analysis of the absorption coefficient and the sound transmission loss, looking for the minimization of sound transmission through a floor system. After some pre-tests, three levels of rubber particles on the mortar mixture and two different rubber particle granulometries were chosen in order to prepare the samples. The experiment was carried out using an impedance tube with the *One Microphone Method* applied to both measurements and the one load method was used for transmission loss determination on a frequency range from 400 Hz to 2500 Hz. Additionally, a floor system with three layers it was simulated to study the system behavior with the rubber addition on the mortar. The results showed an influence of the rubber particle size in the transmission loss, and an improvement of insulation for samples with larger rubber particles for experimental composites and simulated floor systems. It was also studied the mechanical behavior of the new composite, testing the tensile bond strength of composites and comparing them to the pure adhesive mortar sample. Results showed a decrease on bond strength for tested composites.

Keywords: Absorption coefficient, transmission loss, adhesive mortar, scrap tire rubber particles, composite.

List of Figures

List of Tables

Notation

Latin Letters

c	Sound wave speed in air
E	Young's modulus
h	Samples thickness
k	Wave number
$\tilde{K}(\omega)$	Dynamic bulk modulus
$P_{x=0}$	Sound pressure at sample surface
$P_{x=h}$	Sound pressure at sample termination
R_a	Reflection coefficient for anechoic termination
T_a	Transmission coefficient for anechoic termination
TL	Sound Transmission Loss
$V_{x=0}$	Particle velocity at sample surface
$V_{x=h}$	Particle velocity at sample termination
$v(r)$	Microscopic velocity of the fluid in the pore
$v(r_w)$	Velocity of the fluid in the surface pore walls
Z	Characteristic impedance

Greek Letters

α	Absorption coefficient
α_∞	Tortuosity
η	Damping
θ	Sound wave incidence angle
Λ	Viscous characteristic length
Λ'	Thermal characteristic length
μ	Air viscosity
ν	Poisson's ratio
ρ_0	Air density
σ	Air flow resistivity
φ	Porosity

Acronyms

ANIP	Associação Nacional da Indústria de Pneumáticos
BR	Polybutadiene Rubber
CEMPRE	Compromisso Empresarial Para Reciclagem
DSC	Differential Scanning Calorimetry
FRF	Frequency Response Function
FTIR	Fourier Transform Infrared
JCA	Johnson-Champoux-Allard model
SBR	Styrene-Butadiene Rubber
TGA	Thermogravimetric Analysis

Table of Contents

1 Introduction

For many years, control of sound trespassing from one building space to another has been studied and regulated in many countries (Litvin and Belliston, 1978). There are several negative effects from noise exposure, such as lack of comfort, health problems, privacy reduction and sleep disturbance (Paixão, 2002).

Industrial sectors such as automobile, aeronautic, home appliances and even construction have been working on the reduction of noise levels produced by their products or transmitted through them. Some works in the construction field are focused on wall insulation noise produced indoors and outdoors. Despite this, noise originated between buildings floors has become a concern because of the global trend to build apartment buildings instead of single-family houses. This noise comes from two different kinds of sources: impact noise, produced for example by steps and objects falling, and aerial noise, produced for example by talking, TV or radios.

In order to contribute to the noise reduction between floors, the Brazilian Association of Technical Standards (ABNT) included changes in ABNT NBR 15575 “Housing buildings performance”, which establishes criteria for thermal, acoustic, luminous performance, and fire safety. On ABNT NBR 15575-3: 2013 (ABNT 15575, 2013), a floor system is defined as a horizontal or plane system compounded of layers to fulfill structural functions, traffic and sealing. As shown in Figure 1.1, a layer destined to thermal and acoustic insulation is recommended. The development of thermal and acoustic insulation systems in the construction field in Brazil has been increased. Some specific products for this purpose are already available in the Brazilian market (Aubicon, Accessed: November 2015).

Despite having specialized materials for this purpose, most of them made of foams and fibers applied in the 3th layer of the floor system, they cannot guarantee the insulation of a large range of frequencies of the generated noise, however, insulation frequency is not always

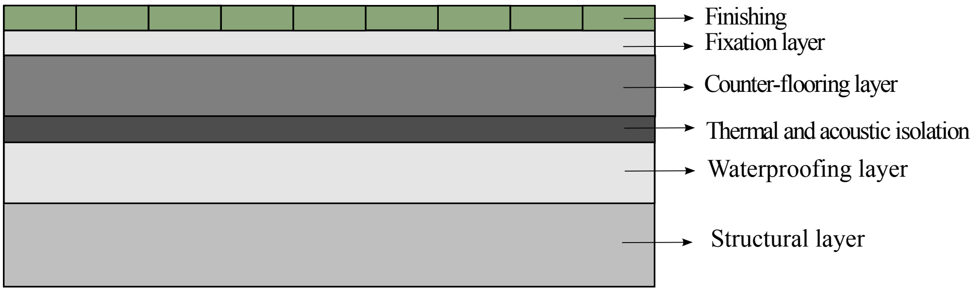

Figure 1.1: Floor system scheme described in ABNT 15575-3 (ABNT 15575, 2013)

the same for airborne or impact noise. In order to enlarge the sound insulation bandwidth for airborne noise, the material used in the *fixation layer*, due to the material's proximity with the source and the facility to absorb direct impacts, can also be acoustically improved.

1.1 Motivation

Tire rubber reuse is currently an environmental concern as every manufactured tire needs to be discarded after their life cycle end (Almeida Júnior et al., 2012). Once discarded, tires are usually stockpiled and that practice causes a negative environmental and health impact, attracting rats, mice and mosquitoes (Elchalakami, 2014).

According to *"Compromisso Empresarial Para Reciclagem"* (CEMPRE), tire milling is one of the recycling alternatives for tire rubber. This process results in the fabrication of recycled products, e.g.: car floor mats, blankets for sports fields, industrial flooring, shoe soles, etc. (CEMPRE, Accessed: March 2016).

In Brazil, the *"Associação Nacional da Indústria de Pneumáticos"* (ANIP) has a program dedicated to the collection of useless tires, RECICLANIP. In 2014 the program collected about 445 thousand tons, which corresponds to 89 million automobile tires. 69.7% of those tires are destined as alternative fuel in the cement industry; the remaining material was shredded and reused mainly as rubber asphalt. One of the ANIP proposals is to stimulate the use of rubber particles resulting from the milling in composites and mixtures in order to contribute to the sustainable production cycle of tires (ANIP, 2015).

Concerned about the scrap tires disposal, the Brazilian environmental institutions created legal instruments (Resolution 416/2009 of the National Environmental Council and Normative Instruction 01/2010 of the Brazilian Institute of Environment and Renewable Natural Resources) that establish that for each new tire sold, tire manufacturers or importers must allocate one scrap tire in an environmentally discarded way using reuse or recycle procedures allowed by the environmental agencies (Pfeifer, 2012; CONAMA, 2012). The Resolution 416/2009 motivated a significant increase of scrap tires recycling in the last decade, and the generated products obtained by the recycling process are being used in several productive sectors. As an example, the rubber particles or aggregates have been used in asphalt blankets, but there is still a high and growing amount of rubber waste available to other sustainable applications/destinations (Pfeifer, 2012).

A possible application for rubber reuse is to make adhesive mortar composites with those rubber particles in order to improve the noise insulation of mortar. Despite the studied application in this work needs the study of transmission loss, and adhesive mortar will not be in the floor surface, it is interesting to study both, absorption and transmission properties in order to characterize the composites where only the airborne noise was considered.

1.2 Related works

A review of related works considering the sound absorption and the sound transmission loss was made.

According to Honorato (Honorato, 2013), when an acoustic wave hits a porous material, there is a relative movement between material phases which causes friction and as a consequence, an energy dissipation, transforming the acoustic energy into thermal energy. This effect is known as *Sound absorption*. On that work, an analytic model evaluation for sound absorption on poroelastic materials was also presented.

Considering the relation of the porosity and the sound absorption, Atalla (Atalla et al., 2001) studied the porosity distribution influence on the acoustic absorption by making a representation of a porous material and controlling the pores distribution. A proper distribution of pores will give better results on sound absorption.

Mafra (Mafra et al., 2005) made a study of a coconut fiber panel compared with commercial panels, absorption coefficient were obtained using the *Transfer Function Method* with an impedance tube. They made the evaluation of the coconut fiber panel by varying the density and thickness, obtaining a better absorption with thicker and denser panels.

The method for measuring the absorption coefficient is mentioned in the ISO 10534-2 (ISO 10534-2, 2001), where the impedance tube is used and the absorption coefficient is computed through the use of the transfer function method.

Some studies about transmission loss of mortar and concrete composites expose a potential application of rubber particles into the adhesive mortar for buildings sound insulation. Litvin (Litvin and Belliston, 1978) studied the insulation of concrete and concrete masonry walls by the transmission loss measurements of test specimens made of concrete and different combinations of furring, and the improvement of the transmission loss with the furring addition was achieved.

The method applied to experimentally measure the transmission loss was studied by Jung (Jung et al., 2008) by the theoretical and experimental definition of the transmission loss (TL) of fibber and foam materials using an impedance tube and the *Transfer Matrix Method*, obtaining a high coherence between theoretical and experimental results.

Sgard and Atalla (Sgard and Atalla, 2000) investigated the modeling of TL of a heterogeneous porous material consisting of a porous material containing particles of a solid material with lower density than the density of the porous material. In this reference, a square panel with 10 cm side and 3.75 cm thickness was considered. The TL was not affected in the low frequency region by the presence of solid particles. But in the high frequency region, the TL of the heterogeneous material was greater than that of the porous material without the solid particles.

Costa (Costa et al., 2005) made a study of different adhesive mortar brands by various manufacturers. The study included a granulometry distribution of those types of adhesive mortar, obtaining that the higher percentages of mortar particles are distributed between 100 μm and 1000 μm (140 mesh to 18 mesh).

Rubberized concrete and mortar composites has been studied and their mechanical properties have been tested. Canova (Canova et al., 2008) made a coating-mortar mechanical properties analysis when adding scrapped tires particles. The composite presented lower incidence of fissures and a reduction on the static deformation modulus and tensile strength. They also observed an increment on the air content into the mortar/rubber composites. Similar studies were made by Elchalakani (Elchalakami, 2014), who added silica fume to rubberized concrete mixed with crumb powder in order to increase the axial compressive strength and the elasticity modulus.

Another work involving rubberized concrete was made by Tunratsinze (Turatsinze and Garros, 2008), where the modulus of elasticity and strain capacity of Self-Compacting Concrete were studied. In this work it was observed a quasi-linear increase in air content as function of rubber aggregates, confirming that the hydrophobic nature of rubber helps to increase the air content when rubber aggregates are added. Earlier studies by Segre (Segre and Joekes, 2000) show that surface treatments with $NaOH$ saturated water solutions on the rubber particles improved the adhesion of rubber into the cement matrix, resulting on a porosity decrease.

Mohamed *et al* (Mohammed et al., 2012), studied the acoustic, thermal and electrical properties of hollow concrete blocks with crumb rubber as a partial replacement to fine aggregate using 0%, 10%, 25% and 50% crumb rubber volume into the samples. They also added silica fume and pulverized fuel ash in order to achieve the mechanical product requirements. As the amount of rubber increased, the density decreased, the air content, thermal resistivity sound absorption and toughness augmented, as well as the impact resistivity. However, it was observed a compressive strength reduction and a water absorption increase. Su *el al.* added different rubber particle sizes into the concrete; it was observed that with smaller particles, workability was improved (Su et al., 2015).

As seen, mechanical and acoustical studies of concrete, masonry and coating mortar composites have been made, however adhesive mortar composites have not been deeply studied, showing a potential application for buildings sound insulation.

1.3 Aim of this work

The main aim of this work is to investigate how the addition of rubber particles affects the acoustic properties of an adhesive mortar commonly used in the floor system of Brazilian buildings. For this purpose, the *absorption coefficient* α and the *transmission loss* TL of mortar/rubber composites were measured and the acoustic behavior was analyzed considering some aspects of the material micro-structure.

Some of the specific aims were:

- To prepare composites with different mortar/rubber particles proportions and different granulometry for acoustic application,
- To analyze the composite micro-structure,
- To obtain the experimental sound absorption coefficient and the transmission loss of the prepared composites with an impedance tube,
- To determine the effect of the rubber particle addition in the mortar adherence.

1.4 Work structure

This work is structured in 5 chapters as described below.

Chapter 2 shows a description of the primary materials used on the adhesive-mortar/rubber-particles samples and its fabrication process. It also includes a morphology and a porosity analysis of the obtained composites.

Chapter 3 describes the properties of interest, *Absorption Coefficient*, *Transmission Loss* and *Adherence* concepts, as well as the applied methods to measure them.

Chapter 4 shows the experimental planning followed to prepare rubber/mortar composites with different ratios and rubber particle granulometry as well as the obtained results for the tested properties.

Finally, the conclusions are presented in Chapter 5.

2 Tested materials

Adhesive mortar for indoor use mixed with scrap tire rubber particles was selected to be studied in this work. Only the airborne noise was considered in order to do an initial study of the composite behavior.

There is a large interest on scrap tire reuse due to its non biodegradable condition, and since buildings have a long life cycle, Scrap tire rubber can be employed as an aggregate in the building systems.

2.1 Adhesive mortar

The adhesive mortar is made of homogeneous mixture of one or more binders with sand and water (Isaia, 2007) its functions are: paste the ceramic tile on the substrate and absorb natural deformations on the ceramic coating system. Some required properties of the adhesive mortar are:

- *Workability:* which is the property on "fresh state" that determines the easiness of mixing, transporting, applying, and finishing of the mortar in a homogeneous condition (Isaia, 2007).
- *Adherence:* this property depends on the interaction between two materials and could be defined by the tensile adherence strength and the shearing adherence strength.

The composite material we are looking for in this work should maintain these properties, ensuring the performance of the mortar in the floor system.

Some of the negative characteristics of mortar are its brittle nature and the low sound absorption, making it a reflective material. This acoustic property could be an advantage to prevent the sound transmission between two rooms as shown in Figure 2.1. Furthermore, when sound waves strike the room's enclosure, they are reflected away generating a problem on room 1 due to the sound reverberation due to the reflection on the walls (Holmes et al., 2014).

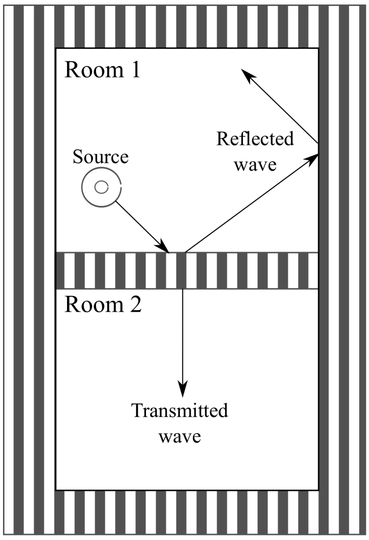

Figure 2.1: Sound waves interaction between two rooms, based on Barron (Barron, 2001)

The adhesive mortar used in this work is classified as AC-I according ABNT NBR 14081-1 (ABNT 14081, 2004), and it contains cement, mineral aggregates and non toxic additives, as described by Usina Fortaleza manufacturer.

2.2 Scrap tire rubber particles

Rubber particles were kindly supplied by Borcol Tapetes Automotivos situated in Sorocaba, São Paulo State, Brazil, and were used as received. It is difficult to know the exact rubber chemical composition because tires can be manufactured with different kinds of organic polymers. Styrene-Butadiene Rubber (SBR) is the most commonly used, but natural rubber (polyisoprene), nitrile rubber, chloroprene rubber and polybutadiene rubber can also be used in tire production (Williams and Besler, 1995).

In order to have some information about the rubber particles used here, they were characterized by Fourier Transform Infrared (FTIR) Spectroscopy, Differential Scanning Calorimetry, and Thermogravimetric Analysis. It was verified that rubber particles contain natural rubber mixed with SBR or polybutadiene rubber (BR), or mixed with both SBR and BR. Further information of the characterization results is shown in Appendix A.

2.3 Mortar/rubber composites

Composites were prepared with different adhesive-mortar/rubber-particle ratios, following an experimental planning described in this Section.

In order to know the particle size distribution on the mortar/rubber composites, rubber particles were separated using different sieve sizes. Two portions of rubber particles were used: the rubber particle portion between 18 and 35 mesh (named M35) and the rubber particle portion between 35 and 60 mesh (named M60).

Mortar/rubber particle composites were prepared using a proportional water amount suggested by the mortar manufacturer (4 l of water to 20 kg of mortar): for 30 g mortar samples, 6 ml of water were added, and for samples with higher rubber particle amounts (25% on mass composition) 6.5 ml of water were used in order to preserve the workability of the wet paste. The mixtures were made in disposable cups. Dry components (adhesive mortar and rubber particles) were initially weighted on a *Sartorius 124S* analytic balance and mixed by hand for 30 seconds.

After the water addition, samples were mixed for another 30 seconds and transferred to wood substrates, which were previously treated with *Desmol CD* oil release agent. It was used a circular mold of 58 mm diameter by 5 mm height in order to obtain the composites with appropriate dimensions for tests in the impedance tube. These samples were characterized as described in sections 2.3.1 and 2.3.2.

In order to determine the rubber addition effect into the mortar absorption coefficient the transmission loss, an experimental planning considering two factors, the *composite composition* and the *rubber particle granulometry*, was performed. Table 2.1 shows the three levels for composition.

Table 2.1: Levels for composition

Level	Mortar (%)	Rubber particles (%)
1	90	10
2	85	15
3	75	25

The second factor is the rubber particle size, having two different levels as shown in Table 2.2.

Table 2.2: Levels for granulometry

Level	Particle size (mesh)	Particle size (μm)
1	$60 - 35$	$250 - 500$
2	$35 - 18$	$500 - 1000$

The number of experiments to combine the levels and factors in this case requires six experiments in total. Table 2.3 shows the 6 possible combinations of the factors and the given name for each sample with the code CXX to represent the XX percentage composition of rubber and the code MYY to represent the YY rubber particle size on mesh.

Table 2.3: Factors combination for samples preparation

Sample	Composition [%] (mortar/rubber)	Granulometry [mesh]	Sample name
1	90/10	60	C10M60
2	90/10	35	C10M35
3	85/15	60	C15M60
4	85/15	35	C15M35
5	75/25	60	C25M60
6	75/25	35	C25M35

Additionally, a *"standard sample"* without rubber particles was made in order to compare the results of the modified mortar with the pure one. Two replicas of each sample were prepared leading to a total of 14 samples.

2.3.1 Micro-structural analysis

After the cure period, the final diameter, thickness and density of samples were measured and are shown on Table 2.4. As composites can be treated as porous materials, measured density is the apparent density, i.e.:

$$\rho_{ap} = \frac{m_r + m_{air}}{V_r + V_{air}} \tag{2.1}$$

where m_r is the solid matrix mass, m_{air} is the air mass into the pores, V_r is the solid matrix volume and V_{air} is the air volume into the pores. When adding rubber particles, the mortar apparent density decreases as the rubber particles amount in composites increases, showing a lower apparent density for composites with 60 mesh rubber particles.

Table 2.4: Samples properties after seven days cure period

Sample	Diameter [mm]	Thickness [mm]	Apparent Density [g/cm^3]
Pure mortar	58.9	5.2	1.51
Pure mortar	59.2	5.2	1.52
C10M60-a	58.0	5.0	1.24
C10M60-b	58.3	5.2	1.25
C10M35-a	58.4	5.4	1.29
C10M35-b	58.3	5.0	1.34
C15M60-a	58.0	5.8	1.08
C15M60-b	57.9	5.4	1.14
C15M35-a	58.0	5.2	1.13
C15M35-b	58.0	5.2	1.20
C25M60-a	57.8	5.4	0.97
C25M60-b	57.8	5.7	0.97
C25M35-a	58.0	5.8	0.92
C25M35-b	57.9	5.8	1.01

To verify the morphology and pores distribution, samples were metallized with gold with a *BAL-TEC SCD-050* metallizer and analyzed with a *ZEISS EV0 MA15* Scanning Electron Microscope, however, the obtained images did not show morphological differences or phase separation, resulting impossible to see the pores distribution. Figure 2.2 shows the obtained images.

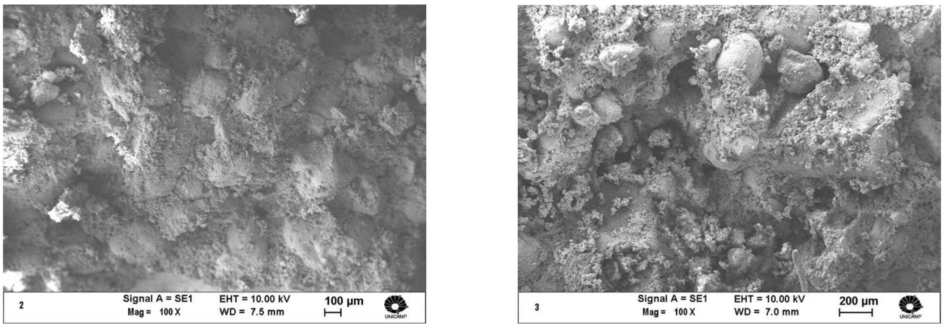

(a) C10M60 (b) C10M35

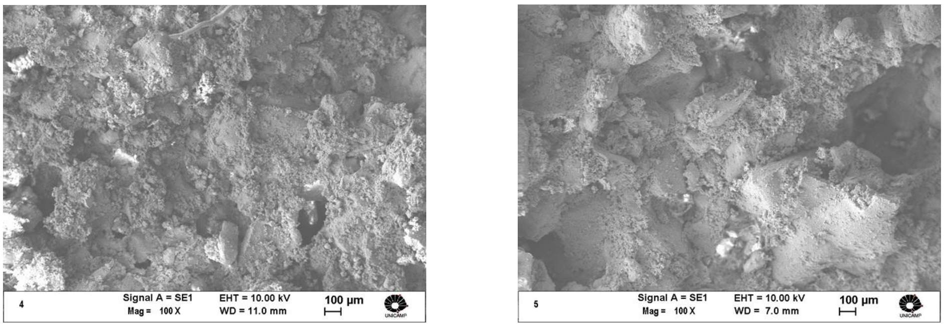

(c) C15M60 (d) C15M35

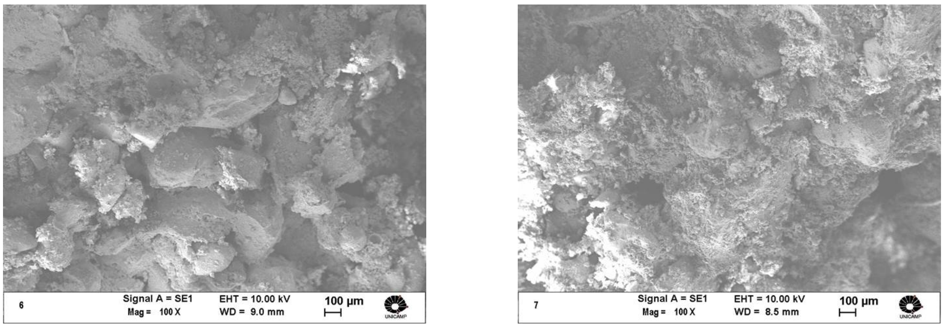

(e) C25M60 (f) C25M35

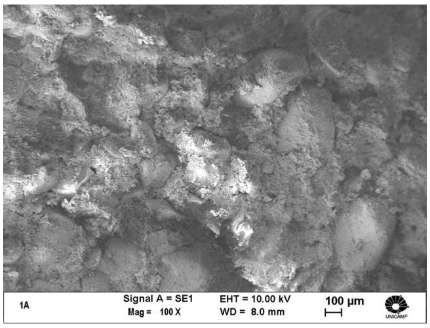

(g) Pure

Figure 2.2: Scanning Electron Microscopy of pure adhesive mortar and mortar/rubber composites

2.3.2 Porosity analysis

In order to have a better resolution and know the sample's porosity, a *Bruker SKYSCAN 1272* X-ray Microtomograph with a 10 μm resolution available at the "Brazilian Nanotechnology National Laboratory (LNNano)" was employed. Samples with dimension of approximately 5 mm×7 mm×5 mm were analyzed and the images were digitally reconstructed, identifying zones with different densities.

Using the ImageJ free processor, five regions of 2 mm^3 for each sample were selected. Considering the software density histogram, regions with the lowest density were defined as "empty spaces", i.e., pores. The volume percentage of pores were computed, allowing to estimate the porosity of the samples. The porosity results are shown in Table 2.5 with the standard deviation range.

Table 2.5: Porosity values estimated from X-ray microtomography images treatment

Sample	Porosity [%]
Pure mortar	25.4±0.8
C10M60	45.0±0.9
C10M35	44.2±0.9
C15M60	57.0±1.0
C15M35	45.8±0.3
C25M60	66.4±0.5
C25M35	60.3±0.4

Representations of these volume regions are shown in Figure 2.3. These images were obtained by using CTan/CTVox/CTVol softwares developed by Bruker. In Figure 2.3, the red regions represent the lowest density domains, the gray regions represent the highest density domains, and the yellow regions represent the domains that have intermediate values of density. The three different regions were selected considering the histogram analysis and they can be related to pores and rubber particles domains in each sample. So, colored regions can represent pores (red regions), rubber particles (yellow regions) and mortar (gray regions).

For mortar/rubber composites, it was possible to observe that lowest density regions (red

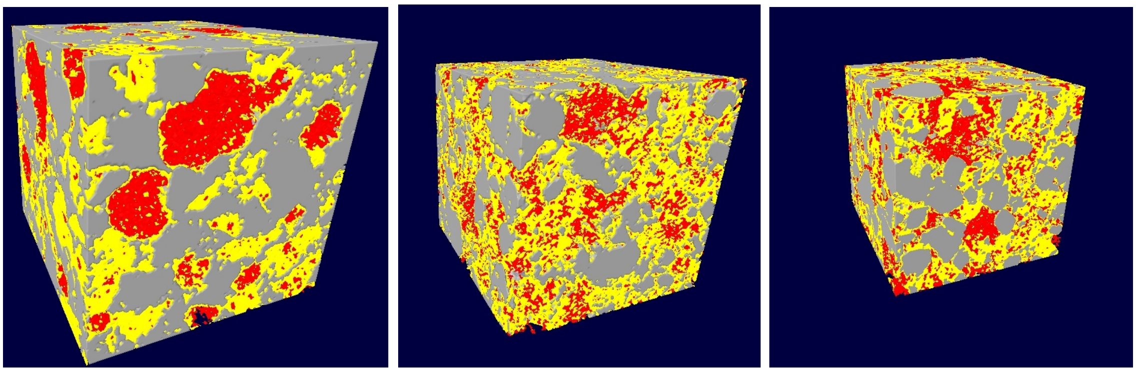

(a) C10M60 (b) C15M60 (c) C25M60

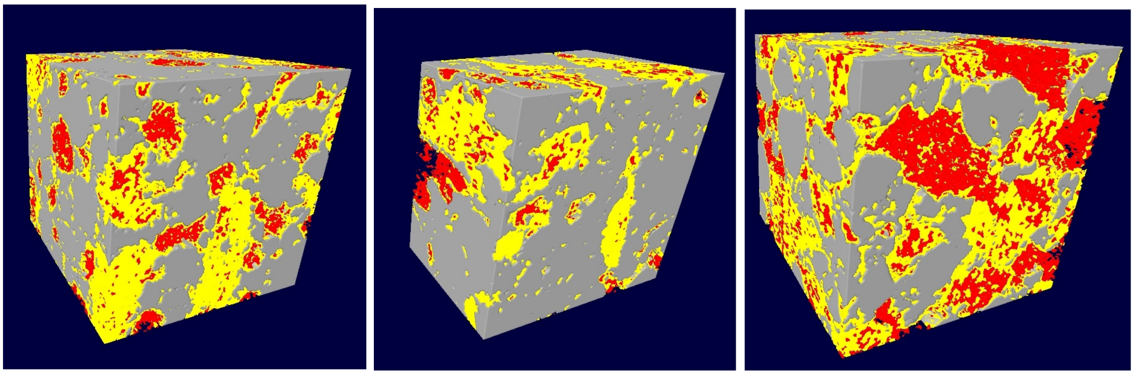

(d) C10M35 (e) C15M35 (f) C25M35

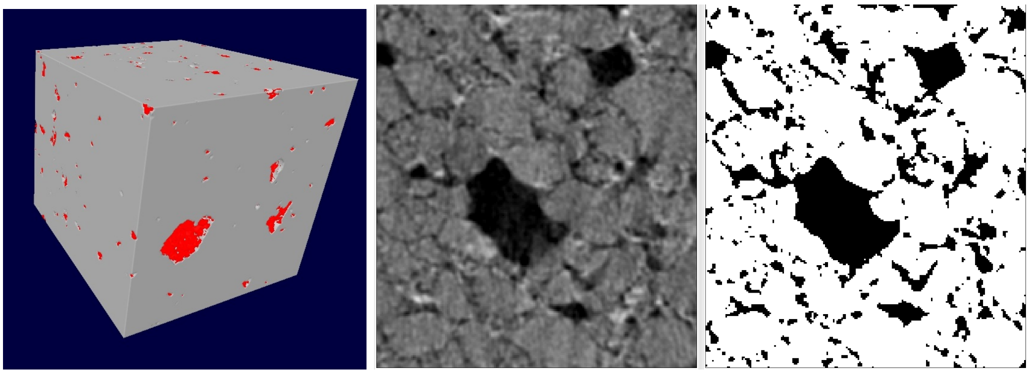

(g) Pure mortar (h) Pure mortar

Figure 2.3: (a) to (g) Representations of volume regions (2 mm by 2 mm by 2 mm) for pure mortar and mortar/rubber composites originated from the treatment of X-ray microtomography images and density histograms. (h) Slice of the X-ray microtomography image for pure mortar showing the slice before (left side) and after (right side) binary processing in Image J sofware

ones) were located into the yellow regions, this effect can be due to the hydrophobic nature of the rubber, creating a separation between rubber particles. It is interesting to note that interfacial regions between the rubber particles and mortar did not present empty spaces: it is not possible to see red regions on the interfacial gray and yellow regions, which represent “pores”, showing a good interaction between the mortar and rubber particles for all composites.

3 Properties of interest

Considering the noise reduction, there are two related concepts: *the sound absorption* and *the sound insulation*. The first one is the material property related to dissipation of an acoustic wave, while the second one is the property related to the rejection of an acoustic wave by its reflection.

As illustrated in Figure 3.1, when a sound wave hits on a barrier of a different material, the energy is divided: one part is transmitted, another is reflected and the last one is absorbed (Barron, 2001).

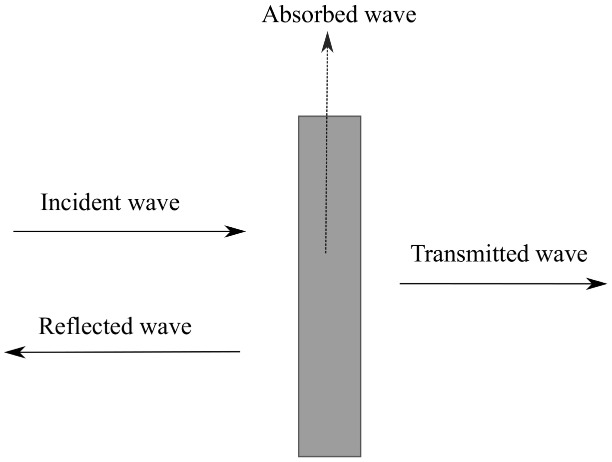

Figure 3.1: Transmission of sound through a barrier according to Barron (Barron, 2001)

The magnitude of each wave (absorbed, reflected and transmitted) can be obtained by calculating their respective coefficients: absorption coefficient α for the absorbed energy, reflection coefficient $|r|^2$ for the reflected energy, and transmission coefficient $|T|^2$ for the transmitted energy.

Figure 3.2 illustrates the properties of interest on each room with the sound source placed in Room 1. Into the source room, the interest is to study the sound absorption, due to the sound reflection caused by the barriers (ceiling, walls and floor). From Room 1 to Room 2, the interest is to study the sound transmission of airborne noise.

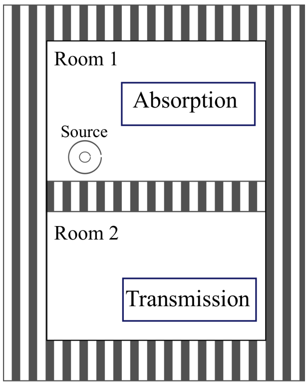

Figure 3.2: Properties of interest on each room

Verification of the Tensile Bond Strength of the mortar/rubber composite was also an interest of this work, in order to know the composites adhesion by tensile pulling and to verify the effect of rubber addition on the adhesion property.

3.1 Experimental method for absorption coefficient determination

According to Barron (Barron, 2001), sound-absorbing materials are used to reduce sound levels or reverberation in a room, acting on the surface striking sound and not on the sound source.

The absorption coefficient α is the ratio of the acoustic energy absorbed to the acoustic energy striking the surface, i.e.,

$$\alpha = \frac{W_{abs}}{W_{in}} \tag{3.1}$$

Despite the fact that the mortar is not located on the surface of the floor system, it is an interest of this work to study the absorption coefficient in order to do a complete characterization and guarantee that this property will not diminish in the composites.

The absorption coefficient and the transmission loss can be measured on the impedance tube device, taking advantage of the plane wave behavior at normal incidence. Another method for these sound properties measurement is using the reverberation chamber. In this case, the chamber size allows to analyze the wave behavior on random incidence, but the sample size should be much bigger than the one used in the impedance tube (Honorato, 2013).

In this work, the impedance tube was chosen as testing equipment due to the facility to do samples of 60 mm of diameter. The equipment employed was an impedance tube *BSWA SW433* of normal incidence with a *source tube*, a *sample holder* and an *extension tube* with 60 mm diameter. The build-in loudspeaker was $4''$ diameter, 20 Watts, 8Ω and a working frequency from 20 Hz to 8000 Hz. Distance from the sample's surface to the microphone 2 was 35 mm, distance between microphones 1 and 2 was 45 mm, and distance between microphones 0 and 2 was 170 mm, see Figure 3.3.

According to the manufacturer, for 125 Hz to 800 Hz measurements, microphones 0 and 2 must be used, and for 400 Hz to 2500 Hz, microphones 1 and 2 must be used. It was used a single microphone on different positions depending on the property to measure and the frequency band to analyze. The signals were processed with a *SIEMENS LMS Test.Lab* FFT analyzer, which generates a random broadband noise and captures the microphone signals, returning the Frequency Response Function (FRF) of each one to the input signal.

For absorption measurements, the sample material is placed at the end of the tube on the sample holder, as shown in Figure 3.3. A plane random wave from 5 to 2560 Hz is emitted through a loudspeaker into the tube traveling to the sample. After hitting the sample, the wave is divided in three parts: the reflected wave, the absorbed wave and the transmitted wave. The last one is considered null due to the rigid wall at the end of the tube, resting the incident wave **A** and the reflected wave **B**.

Waves **A** and **B** are measured by two microphones placed on two fixed positions. Nevertheless according to the ISO 10534-2 standard, the test can be done by using only one microphone, changing its position and sealing the empty holes (ISO 10534-2, 2001).

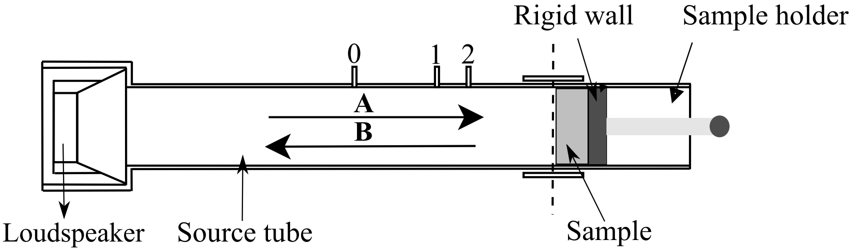

Figure 3.3: Scheme of the impedance tube for absorption coefficient measurement (Bolton et al., 2007)

The transfer function method was applied to determine the absorption coefficient of the material. The tube setup was according to Figure 3.3, with a broadband of 400 Hz - 2500 Hz, which was obtained by introducing the microphone on a fixed position.

Once obtained the FRF from the FFT analyzer, it was possible to obtain the FRF transfer function H_{12} from measured pressures of microphone positions 1 and 2 respectively.

Besides the FRF, it is necessary to calculate the sound speed in the air and the wave number, i.e.,

$$c = \sqrt{\gamma R T} \tag{3.2}$$

$$k = \omega / c \tag{3.3}$$

where c is the sound speed [m/s], γ the specific heat ratio [dimensionless], R is the ideal gas constant for dry air [J/(kg°K)], T is Kelvin temperature [°K], k is the wave number [m^{-1}] and ω is the angular frequency [rad/s].

The sound pressures of the incident wave P_i and the reflected wave P_r can be written as:

$$P_i = Ae^{j(\omega t - kx)} \tag{3.4}$$

$$P_r = Be^{j(\omega t + kx)} \tag{3.5}$$

where A is the incident wave amplitude $[N/m^2]$, B is the reflected wave amplitude $[N/m^2]$, and

x is the distance between the microphone and the sample's surface.

Then, the pressure on each microphone is expressed as:

$$P_1 = e^{j\omega t}(A\,e^{-jkx_1} + B\,e^{jkx_1}) \tag{3.6a}$$

$$P_2 = e^{j\omega t}(A\,e^{-jkx_2} + B\,e^{jkx_2}) \tag{3.6b}$$

where P_1 is the pressure from the microphone on position 1, P_2 is the pressure on position 2, x_1 is the distance between the microphone 1 and the sample's surface and x_2 is the distance from the microphone 2 to the sample's surface.

With the pressures, it is possible to obtain the transfer function between microphone positions 1 and 2 according to the ISO 10534-2 standard (ISO 10534-2, 2001):

$$H_{12} = \frac{H_{F2}}{H_{F1}} \tag{3.7}$$

where H_{12} is the transfer function between signals 1 and 2, H_{F1} is the FRF between microphone 1 and the wave generator, H_{F2} is the FRF between microphone 2 and the wave generator. In this case,

$$H_{12} = \frac{P_2}{P_1} = \frac{A\,e^{-jkx_2} + B\,e^{jkx_2}}{A\,e^{-jkx_1} + B\,e^{jkx_1}} \tag{3.8}$$

With the transfer function determined, the complex reflection coefficient r is calculated as the ratio between the reflected wave's pressure amplitude B and the incident wave's pressure amplitude A, i.e., $\left(r = \frac{B}{A}\right)$. Dividing the terms of Equation (3.8) by A it is obtained:

$$H_{12} = \frac{e^{-jkx_2} + \frac{B}{A}e^{jkx_2}}{e^{-jkx_1} + \frac{B}{A}e^{jkx_1}} \tag{3.9}$$

and $\frac{B}{A}$ can be writen as:

$$\frac{B}{A} = \frac{H_{12} - e^{-jkx_2}}{e^{jkx_2} - H_{12}} \tag{3.10}$$

Therefore the complex reflection coefficient is:

$$r = \left(\frac{H_{12} - e^{-jks}}{e^{jks} - H_{12}} \right) e^{2jkx_1} \tag{3.11}$$

where s is the distance between microphones ($s = x_1 - x_2$), x_1 is the distance between the microphone 1 and the sample's surface and x_2 is the distance from the microphone 2 to the sample's surface.

Applying the energy conservation, the sum of the absorption, energy reflection and energy transmission coefficients must be one. As α is a magnitude which does not contain phase information, energy reflection and transmission coefficients ($|r|^2$ and $|T|^2$) are used instead of complex coefficients (r and T), i.e.,

$$1 = |r|^2 + |T|^2 + \alpha \tag{3.12}$$

However, in the experimental configuration, there is a rigid wall right after the sample, making null the transmission coefficient. In this case, the absorption coefficient is obtained as

$$\alpha = 1 - |r|^2 \tag{3.13}$$

Sound absorption can be explained as the conversion of sound energy into heat due to the interaction between solid (porous structure) and fluid (fluid into the pores, commonly air) phases of a porous material. Best absorbents are highly porous (more than 90%) and the absorption coefficient is near 1 in a wide frequency band.

Pure mortar and mortar/rubber composites can be considered, to a greater or lesser extent, heterogeneous porous materials. In the literature, there are many works dealing with investigation of the acoustic behavior of porous materials, mainly involving the development of analytical models to predict and optimize the acoustic properties for applications in noise control (Khan, 2008). The analytical models are based on macroscopic parameters such as porosity, flow resistivity, tortuosity, viscous and thermal characteristics lengths, and viscous and thermal permeabilities. These models consider that porous material comprises a rigid or elastic matrix, saturated with a fluid, in this case atmospheric air. The model complexity is directly related to the complexity of the shape of the pores. The more irregular the form, the greater the number of macroscopic parameters used in the model to adequately describe the acoustic behavior and sound absorption material. Among the various existing analytical models, perhaps the model of Johnson-Champoux-Allard (JCA) (Johnson et al., 1987; Champoux and Allard, 1991; APMR, Accessed: April 2016) is the most used.

Before analyzing the parameters and experimental curves, it is important to keep in mind what the parameters represent. According to the mathematical modeling of porous absorbents, porosity parameter gives the fractional amount of air (or fluid) volume within the absorbent, and it is a ratio of the total pore volume to the total volume of the absorbent (Cox and D'Antonio, 2006; Mareze, 2013). Porosity is a key parameter and it is directly related with the sound absorption coefficient, i.e., the nearest the porosity to one, the greater the sound absorption coefficient over a large frequency range (Cox and D'Antonio, 2006; Mareze, 2013).

Tortuosity parameter represents the effect of pores orientation relative to the incident sound field on the sound propagation (Cox and D'Antonio, 2006; Mareze, 2013). The more complex the propagation path through the absorbent material, the higher the absorption (Cox and D'Antonio, 2006; Mareze, 2013). The complexity of the path is partly represented by the tortuosity, which affects how easily sound can penetrate the absorbent (Cox and D'Antonio, 2006; Mareze, 2013). Tortuosity changes the frequency region where the maximum in absorption occurs, and in general, when tortuosity increases, the maximum absorption frequency decreases.

Flow Resistivity parameter measures how easily air (or fluid) can penetrate a porous absorbent and the resistance that air flow (or fluid flow) meets through a structure (Cox and D'Antonio, 2006; Mareze, 2013). This parameter affects the absorption curve versus frequency of a more complex way than the porosity. In studies of hypothetical materials where it is considered that the other parameters are fixed, the variation of the flow resistivity is as follows: in the region of low frequencies, the higher the value of the flow resistivity, the greater the absorption. With increasing frequency, there is a reverse effect, i.e., lower flow resistivity lead to higher α values, but this occurs until a certain limit of flow resistivity. When the flow resistivity decreases to beyond the threshold value, the absorption decreases again (Mareze, 2013). Some authors consider the flow resistivity as being the most important parameter in the determination of acoustical properties of porous absorbents (Cox and D'Antonio, 2006).

Viscous and thermal characteristic lengths are related to pore size and shape. The viscous characteristic length is defined as a weighted ratio of the volume to surface area of the pores (Cox and D'Antonio, 2006; Mareze, 2013). It is weighted according to the squared modulus of the microscopic velocity evaluated, including the viscosity effects. The thermal characteristic length is the ratio of the volume to surface area of the pores, without weighting for microscopic velocity (Cox and D'Antonio, 2006; Mareze, 2013).

Johnson (Johnson et al., 1987) proposed a model to describe the complex density of an acoustical porous material $\tilde{\rho}(\omega)$ with a motionless matrix having arbitrary pore shapes:

$$\tilde{\rho}(\omega) = \frac{\alpha_\infty \rho_0}{\varphi} \left[1 + \frac{\sigma\varphi}{j\omega\rho_0\alpha_\infty} \sqrt{1 + j\frac{4\alpha_\infty^2 \mu \rho_0 \omega}{\sigma^2 \Lambda^2 \varphi^2}} \right] \tag{3.14}$$

where ω is the angular frequency of excitation, μ is the fluid viscosity into the pore and ρ_0 is the fluid density, α_∞ is the tortuosity, φ is the porosity, σ is the flow resistivity and Λ is the viscous characteristic length defined as:

$$\Lambda = 2\frac{\int\limits_V |v(r)|^2 dV}{\int\limits_A |v(r_w)|^2 dA} \tag{3.15}$$

where $v(r)$ is the microscopic velocity of the fluid in the pore, V is the pore volume, A is the pore walls surface area and $v(r_w)$ is the velocity of the fluid in the surface pore walls. As seen, Λ is not dependent on the fluid characteristics but on the pore geometry (Champoux and Allard, 1991).

Initially, Johnson's model considered a Newtonian fluid, incompressible on the pore size scale (Champoux and Allard, 1991). However, for fluids as air, a temperature influence over the dynamic tortuosity is verified, and bulk modulus must be obtained from the dynamic tortuosity.

From Champoux-Allard's work, it was added a thermal characteristic length into the Johnson's model. This quantity is defined as:

$$\Lambda' = 2\frac{\int\limits_V dV}{\int\limits_A dA} \tag{3.16}$$

Equations (3.15) and (3.16) are similar, except that thermal effect is not weighted by the local microscopic velocities, then Λ' is twice the volume to pore surface ratio (Champoux and Allard, 1991).

In order to obtain the dynamic bulk modulus, it is necessary to relate Λ and Λ' with the other non acoustic parameters ($\sigma, \varphi, \alpha_\infty, \mu$) as:

$$\Lambda = c\sqrt{\frac{8\alpha_\infty \mu}{\sigma\varphi}} \tag{3.17a}$$

$$\Lambda' = c'\sqrt{\frac{8\alpha_\infty \mu}{\sigma\varphi}} \tag{3.17b}$$

where c and c' are parameters that depend on the geometry of the pores and typically lies between 1 and $1/4$.

Thus, the dynamic bulk modulus ($\tilde{K}(\omega)$) can be obtained as (APMR, Accessed: April

2016):

$$\tilde{K}(\omega) = \frac{\gamma P_0/\varphi}{\gamma - (\gamma - 1)\left[1 - j\frac{8\kappa}{\Lambda'^2 C_p \rho_0 \omega}\sqrt{1 + j\frac{\Lambda'^2 C_p \rho_0 \omega}{16\kappa}}\right]^{-1}} \tag{3.18}$$

where Λ' is the thermal characteristic length, γ is the fluid specific heat ratio, C_p is the specific heat of air at constant pressure, P_0 is the air equilibrium pressure and κ is the thermal conductivity of air.

Through the complex density and dynamical bulk modulus, it is possible to predict the characteristic impedance Z of the porous media as (Khan, 2008):

$$Z = \sqrt{\tilde{\rho}\tilde{K}}\ coth(kh) \tag{3.19}$$

where k is the wave number obtained as $k = i\omega\sqrt{\frac{\tilde{\rho}}{\tilde{K}}}$ and h is the sample thickness.

Finally, the absorption coefficient can be calculated as:

$$\alpha = 1 - \left|\frac{Z - \rho_0 c_0}{Z + \rho_0 c_0}\right|^2 \tag{3.20}$$

where c_0 is the sound wave velocity in air.

3.2 Experimental method for transmission loss determination

The *sound power transmission coefficient* $|T|^2$ is defined as the ratio between the energy transmitted through the wall and the incident energy on that wall:

$$a_t = \frac{W_{tr}}{W_{in}} = |T|^2 \tag{3.21}$$

where W_{tr} is the transmitted power and W_{in} is the incident power.

The transmission loss (TL) is another way to evaluate the transmission of sound. It is expressed and calculated over a range of frequencies by

$$TL = 10\,log\left(\frac{W_{in}}{W_{tr}}\right) \tag{3.22}$$

Thus, the transmission loss will give the quantity of sound (on dB) which is not transmitted from one room to the other.

TL behavior can be explained by considering the transmission of sound through a panel or wall. As described in literature (Barron, 2001; Norton and Karczub, 2003; Munjal, 2013; Gerges, 2000) TL curve could be separated in four regions:

1. the stiffness controlled region, that occurs for low frequencies or for thin panels which vibrates with the acoustic wave. For this region, TL for normal incidence can be described as follows (Barron, 2001):

   $$TL = 10log_{10}(1 + K_s^{-2}) \tag{3.23}$$

   where

   $$K_s = 4\pi f \rho_0 c C_s \tag{3.24}$$

   and C_s for circular panels is:

   $$C_s = \frac{3D^4(1-\nu^2)}{256Eh^3} \tag{3.25}$$

   with D corresponding to the diameter of the panel or wall, h is the thickness, ν is the Poisson's ratio of the panel material, ρ_0 is the air density (or density of the fluid around the panel), c is the sound velocity in the air (or in the fluid around the panel), E is the Young's Modulus and f is the frequency. According to Equation (3.23), TL drops 6 dB for doubling the frequency (Gerges, 2000).

2. the damping controlled region, which is characterized by more than one resonance troughs and is located between the stiffness and the mass controlled regions. In this region TL tends to zero (Gerges, 2000). The lowest resonant frequency marks the transition

between the stiffness controlled region and the mass controlled region. The resonant frequencies are a function of the panel dimensions. For a circular panel of diameter D and thickness h, the first resonant frequency can be obtained by (Barron, 2001):

$$f_{r1} = \frac{10.2 c_l h}{\pi\sqrt{3}D^2} \tag{3.26}$$

where f_{r1} is the first resonant frequency, c_l is the speed of longitudinal sound waves in the solid panel material, and it is estimated from:

$$c_l = \sqrt{\frac{E}{\rho_w(1-\nu^2)}} \tag{3.27}$$

where E is the Young Modulus, ρ_w is the wall density, and ν is the Poisson's ratio of the panel material;

3. the mass controlled region, influenced by the panel surface mass. For this region, TL can be described as following (Gerges, 2000):

   $$TL = 20\ log(Mf) - 47.4 \tag{3.28}$$

   where M represents the panel mass per unit surface. According to Equation (3.28), transmission loss increases 6 dB per frequency octave; and

4. the coincidence region, which is also damping controlled. The critical frequency f_c is given by the following expression (Barron, 2001):

   $$f_c = \frac{\sqrt{3}c^2}{\pi c_l h} \tag{3.29}$$

   where c is the speed of sound waves in the air, and h is the panel thickness. The four regions are observed in Figure 3.4.

The TL can be measured using the impedance tube device by preserving the same princi-

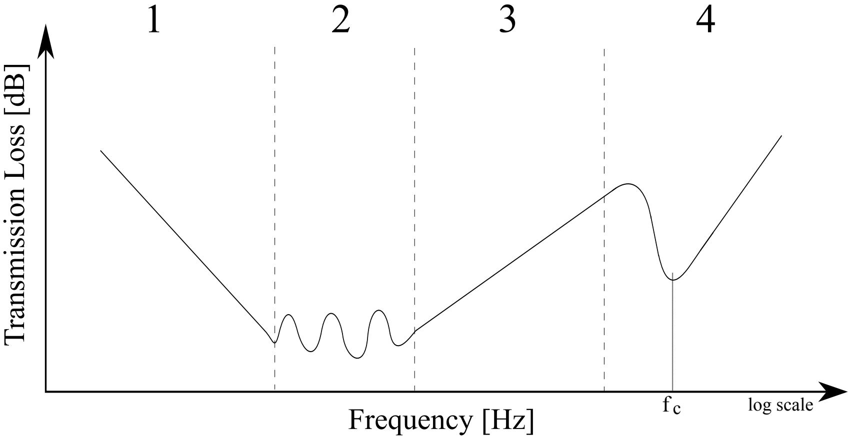

Figure 3.4: Typical TL curve for a wall showing the four regions: 1 Stiffness controlled, 2 Damping controlled, 3 Mass controlled and 4 Coincidence controlled (Munjal, 2013)

ple described for absorption coefficient determination. The difference between the techniques is based on the tube's setting, placing the sample on the middle of the tube to form two chambers with a pair of microphones on each one as shown in Figure 3.5, where the distance from the sample surface to microphone 3 was 100 mm, the distance between microphones 3 and 4 was 45 mm and the distance between 3 and 9 was 170 mm.

After a random wave is emitted by the loudspeaker, there are 4 waves into the impedance tube as shown in Figure 3.5. On the chamber a, wave **A** represents the incident wave and **B** is the reflected wave. On the chamber b, wave **C** is the transmitted wave and wave **D** is the reflected wave by the tube's termination.

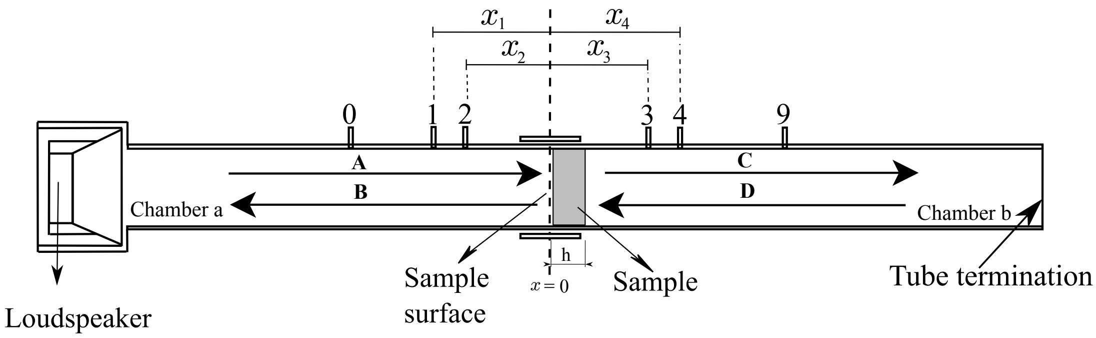

Figure 3.5: Impedance tube scheme for transmission loss measurement (Bolton et al., 2007)

For TL determination, the matrix function method (Bolton et al., 2007) can be applied.

In this case, the tube's setting to measure transmission loss shown in Figure 3.5 implies the formation of two chambers into the tube, ensuring sound pressure and particle velocity on each side of the sample. For this setting, microphone's positions for a broadband frequency range from 400 Hz to 2560 Hz are 1, 2, 3 and 4.

Since it is not possible to experimentally built a completely anechoic termination for the tube, reflection and transmission coefficients can not be simply calculated as $R = B/A$ and $T = C/A$. Instead of this, it is necessary to determine them through the transfer matrix components.

The target of this method is to obtain the components of matrix T that relates the sound pressure P and the particle velocity V for $x = 0$ and $x = h$, sample's thickness h, according to:

$$\begin{Bmatrix} P \\ V \end{Bmatrix}_{x=0} = \underbrace{\begin{bmatrix} T_{11} & T_{12} \\ T_{21} & T_{22} \end{bmatrix}}_{\mathbf{T}} \begin{Bmatrix} P \\ V \end{Bmatrix}_{x=h} \tag{3.30}$$

The sound pressure on each chamber, with P_a the pressure on chamber a and P_b the pressure on chamber b, are

$$P_a = Ae^{-jkx} + Be^{jkx} \tag{3.31a}$$

$$P_b = Ce^{-jkx} + De^{jkx} \tag{3.31b}$$

If the tested positions are 1, 2, 3 e 4, the pressure on each microphone position is:

$$P_1 = Ae^{-jkx_1} + Be^{jkx_1} \tag{3.32a}$$

$$P_2 = Ae^{-jkx_2} + Be^{jkx_2} \tag{3.32b}$$

$$P_3 = Ce^{-jkx_3} + De^{jkx_3} \tag{3.32c}$$

$$P_4 = Ce^{-jkx_4} + De^{jkx_4} \tag{3.32d}$$

where A, B, C and D are the wave pressure amplitudes, x_1, x_2, x_3 and x_4 are the distances between each microphone and the sample surface.

Each wave pressure amplitude can be obtained solving equations (3.32):

$$A = \frac{j(P_1e^{jkx_2} - P_2e^{jkx_1})}{2sin(k(x_1 - x_2))} \tag{3.33a}$$

$$B = \frac{j(P_2e^{-jkx_1} - P_1e^{-jkx_2})}{2sin(k(x_1 - x_2))} \tag{3.33b}$$

$$C = \frac{j(P_3e^{jkx_4} - P_4e^{jkx_3})}{2sin(k(x_3 - x_4))} \tag{3.33c}$$

$$D = \frac{j(P_4e^{-jkx_3} - P_3e^{-jkx_4})}{2sin(k(x_3 - x_4))} \tag{3.33d}$$

Pressures and velocities can be expressed as:

$$P_{x=0} = A + B \tag{3.34}$$

$$V_{x=0} = \frac{A - B}{\rho_0 c} \tag{3.35}$$

$$P_{x=d} = Ce^{-jkd} + De^{jkd} \tag{3.36}$$

$$V_{x=d} = \frac{Ce^{-jkd} - De^{jkd}}{\rho_0 c} \tag{3.37}$$

where P_0 is the atmospheric pressure, and ρ_0 is the air density obtained as:

$$\rho_0 = \frac{P_0}{RT} \tag{3.38}$$

The obtained system of equations has two equations and four variables. The *one load method* (Bolton et al., 2007) can be employed to solve it. This method takes advantage of the reciprocal nature of the sample, which means that the TL is the same on both sides of the sample, implying that the determinant of matrix T must be 1, i.e.,

$$det(\boldsymbol{T}) = T_{11}T_{22} - T_{12}T_{21} = 1 \tag{3.39}$$

where $T_{11} = T_{22}$ because the complex reflection coefficient on both samples surfaces is the same.

Then, the elements of matrix **T** are:

$$\begin{bmatrix} T_{11} & T_{12} \\ T_{21} & T_{22} \end{bmatrix} = a \begin{bmatrix} P_{x=d}V_{x=d} + P_{x=0}V_{x=0} & P_{x=0}^2 P_{x=d}^2 \\ V_{x=0}^2 V_{x=d}^2 & P_{x=d}V_{x=d} + P_{x=0}V_{x=0} \end{bmatrix} \tag{3.40}$$

where:

$$a = \frac{1}{P_{x=0}V_{x=d} + P_{x=d}V_{x=0}} \tag{3.41}$$

Assuming the tube's anechoic termination, the wave amplitude D should be 0, leading to $A = 1$. In this case,

$$P_{x=0} = 1 + R_a \tag{3.42}$$

$$V_{x=0} = \frac{1 - R_a}{\rho_0 c} \tag{3.43}$$

$$P_{x=d} = Te^{-jkd} \tag{3.44}$$

$$V_{x=d} = \frac{Te^{-jkd}}{\rho_0 c} \tag{3.45}$$

Finally, the Equation (3.30) is rewritten as:

$$\begin{Bmatrix} 1 + R_a \\ \frac{1-R_a}{\rho_0 c} \end{Bmatrix} = \begin{bmatrix} T_{11} & T_{12} \\ T_{21} & T_{22} \end{bmatrix} \begin{Bmatrix} Te^{-jkd} \\ \frac{Te^{-jkd}}{\rho_0 c} \end{Bmatrix} \tag{3.46}$$

The measured Frequency Response Functions (FRFs) are the relations of the wave pressures P_1, P_2, P_3 and P_4 to the reference signal, generating the transfer functions H_{r1}, H_{r2}, H_{r3} and H_{r4}. In order to obtain the microphones pressures, Equation (3.33) is divided by the reference pressure P_r, which is obtained through the reference *auto-spectrum*, given by

$$G_{rr} = S_x S'_x \tag{3.47}$$

where G_{rr} is the reference auto-spectrum $[Pa^2]$, S_x is the reference signal spectrum and S'_x is the spectrum conjugate and $P_r = \sqrt{G_{rr}}$.

Then, Equation (3.33) can be written as:

$$A = \sqrt{G_{rr}} \frac{j(H_{r1}e^{jkx_2} - H_{r2}e^{jkx_1})}{2sin(k(x_1 - x_2))} \tag{3.48a}$$

$$B = \sqrt{G_{rr}} \frac{j(H_{r2}e^{-jkx_1} - H_{r1}e^{-jkx_2})}{2sin(k(x_1 - x_2))} \tag{3.48b}$$

$$C = \sqrt{G_{rr}} \frac{j(H_{r3}e^{jkx_4} - H_{r4}e^{jkx_3})}{2sin(k(x_3 - x_4))} \tag{3.48c}$$

$$D = \sqrt{G_{rr}}\frac{j(H_{r4}e^{-jkx_3} - H_{r3}e^{-jkx_4})}{2sin(k(x_3 - x_4))} \tag{3.48d}$$

where H_{r1} is the FRF of microphone 1 and reference signal, H_{r2} is the FRF of microphone 2 and reference signal, H_{r3} is the FRF of microphone 3 and reference signal, H_{r4} is the FRF of microphone 4 and reference signal.

With the transfer matrix components determined, the complex reflection coefficient R_a and the complex transmission coefficient at normal incidence T_a are calculated:

$$T_a = \frac{2e^{jkd}}{T_{11} + \frac{T_{12}}{\rho_0 c} + T_{21}\rho_0 c + T_{22}} \tag{3.49}$$

$$R_a = \frac{T_{11} + \frac{T_{12}}{\rho_0 c} - T_{21}\rho_0 c - T_{22}}{T_{11} + \frac{T_{12}}{\rho_0 c} + T_{21}\rho_0 c + T_{22}} \tag{3.50}$$

and the TL is calculated as:

$$TL = 10log\left(\frac{1}{|T|^2}\right) \tag{3.51}$$

An algorithm for TL obtainment from experimental data was developed using Matlab and is presented in Appendix B.

3.3 Predicting the Transmission Loss

A variation of the Transfer Matrix Method is applied in the TMTX software (Tanneau et al., 2006) used to simulate a floor system due to the interest of knowing the TL variation of floor systems using the mortar/rubber composite material. This software simulates a multilayer system with finite thickness in Z axis and infinite dimensions in X and Y axis where plane waves are propagated (Tanneau et al., 2006). TMTX allows the study of solid isotropic materials, fluid layers and porous material layers.

The software can represent a system with N layers with thickness h, where layer 1 and N represent the incident and the receptor medium, in this case, air. Assuming a plane wave propagating in the system with an incident angle θ_i, a wave number k_i and an amplitude ϕ_i, a reflected wave to the i medium and a transmitted wave trough the $i+1$ medium on each interface $(i, i+1)$ are presented in Figure 3.6.

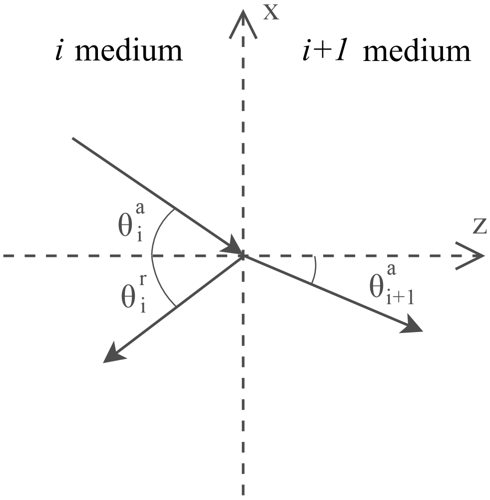

Figure 3.6: Waves behavior in a multilayer system interface (Tanneau et al., 2006)

Then, the wave equation for a point M belonging to the i layer is:

$$\phi_i(M) = (\phi_i^a e^{-jk_i z cos(\theta_i)} + \phi_i^r e^{jk_i z cos\theta_i})e^{-jk_i x sin\theta_i} \tag{3.52}$$

In this case, due to the normal incidence, $\theta_i = 0$ thus, wave equation is written as:

$$\phi_i(M) = \phi_i^a e^{-jk_i z} + \phi_i^r e^{jk_i z} \tag{3.53}$$

The software uses the material properties to find, at each layer interface, the continuity relations in a border point M in order to obtain the incident and transmitted wave amplitudes ϕ_N^a and ϕ_1^a respectively, and thus calculate the energy transmission coefficient.

$$|T|^2 = \frac{\rho_N |\phi_N^a|^2}{\rho_1 |\phi_1^a|^2} \tag{3.54}$$

3.4 Tensile Bond Strength determination

The tensile bond strength test, in order to know the mortar adhesion by tensile pulling, is regulated by ABNT NBR 14082 standard (ABNT 14084, 2004).

A concrete substrate must be previously fabricated with specified parameters according to ABNT NBR 14082 standard (ABNT 14082, 2004). For comparison purposes, it is important to have concrete substrates with the same characteristics.

For the 35×60×5 cm slabs fabrication, three steel grids with 5 mm diameter and 10 cm spacing, Portland cement type CPV ARI and coarse aggregates were used. In addition, three wooden molds to melt the concrete were made, as shown in Figure 3.7 (b).

Cement, sand, aggregates and water were mixed on a concrete-mixer with a 1:2:1:1.6 (cement : sand : aggregates : water) proportion. Half of the mold was filled with the mixture, then the steel grid was placed into the mold which was totally filled. The slabs were laid on a room for a 28 days cure period. Figure 3.7 ilustrates the substrate's fabrication process.

After the cure period, the adhesive-mortar/rubber-particles composites were extended in the longitudinal direction on the standard concrete substrate as shown in Figure 3.8 (Costa et al., 2005). Grooves were plotted on the longitudinal direction with the float trowel. Ten 5×5 cm ceramic pieces were placed on the mortar and mortar/rubber composites. The ceramic pieces were arranged in order to have a spacing of 5 cm between them and a minimum of 2.5 cm to the border.

These sets were also laid on a room for 28 days. Steel pieces were glued with epoxy glue and laid for cure 72 hours before the test. Complete set is shown in Figure 3.9.

The test was executed with a *SCHENCK* machine and a *HBM load cell*. The experimental setup is shown in Figure 3.10.

(a) Material's mixing (b) Concrete distribution on the mold (c) Grid addition

(d) Mold filling (e) Slab finishing

Figure 3.7: Concrete substrates fabrication

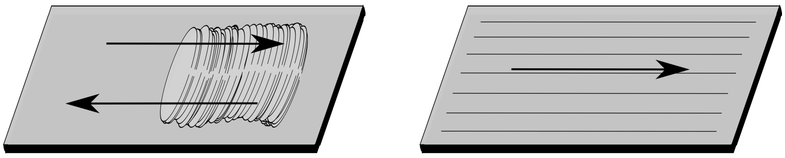

(a) Mortar application on the substrate (b) Grooves formation direction

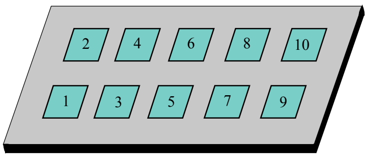

(c) ceramic pieces arrangement

Figure 3.8: Mortar application on substrate and ceramic pieces distribution based on (Costa et al., 2005)

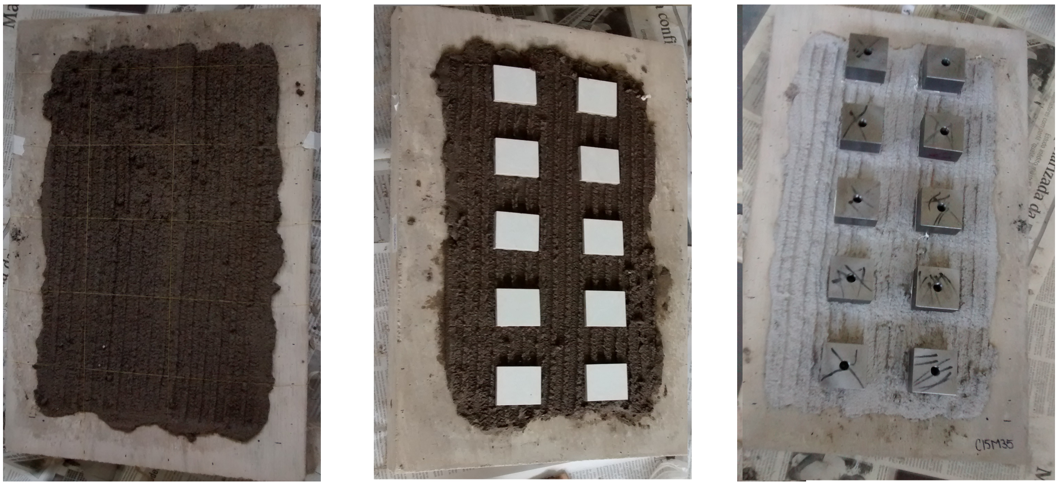

(a) Mortar application and guides for ceramic placement

(b) ceramic pieces arrangement

(c) Tensile bond strength test set

Figure 3.9: Set preparation for tensile bond strength test

Figure 3.10: Experimental setup of Pure sample

4 Results

The measurement of absorption coefficient and transmission loss were performed for high frequencies, from 400 Hz to 2500 Hz with a 5 Hz resolution (BSWA Tech, 2010).

4.1 Absorption coefficient

To show the absorption results, the mean for each sample's replicas was computed, then two figures are presented in order to analyze the effect of each factor into the absorption coefficient α.

Figure 4.1 shows the behavior of α for pure mortar and for mortar/rubber composites. Compared to the pure sample, both rubber/mortar composites (C25M60 and C25M35), have a higher absorption over all the investigated frequency range. It is also seen that composites and pure mortar do not show a high absorption, i.e. for most of the samples α is between 0.1 and 0.2. The composite containing 25% of rubber particles shows a better absorption coefficient for the thinner rubber particles on frequencies higher than 1200 Hz.

According to Doutres (Doutres et al., 2010), there are three groups of classical methods to evaluate the five non-acoustic properties of porous materials on the JCA model:

1. The direct methods, based on the physical definition of the searched property, in this case, measurement of all non-acoustical properties is not straightforward because one dedicated setup per property is required;
2. The indirect methods, based on the acoustical model from which analytical expressions linking the material non-acoustic properties to acoustical measurements are derived. This method needs two intrinsic acoustic properties of the material, such as the effective density $\tilde{\rho}$ and the effective bulk modulus $\tilde{K}$, usually obtained with an impedance tube setup

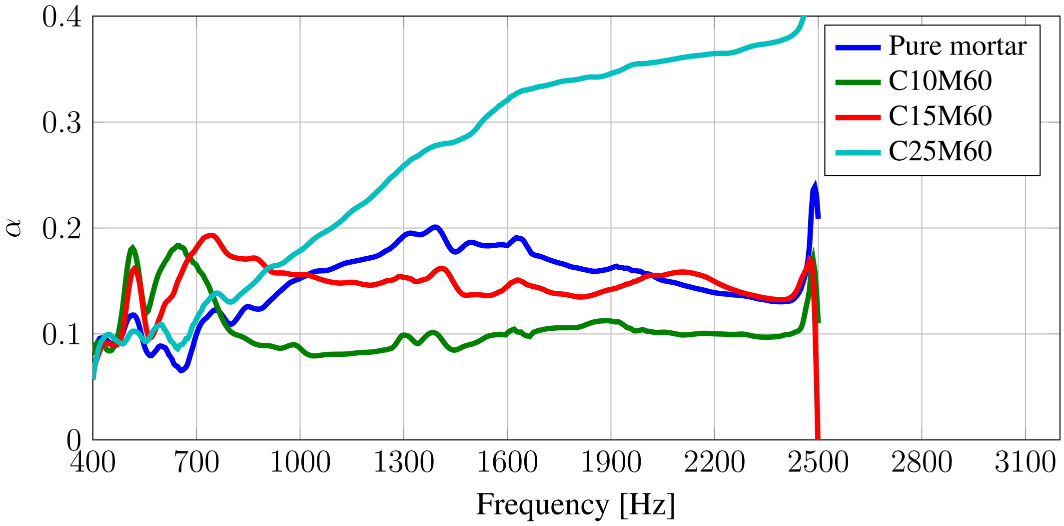

(a) Absorption coefficient for 60 mesh composites

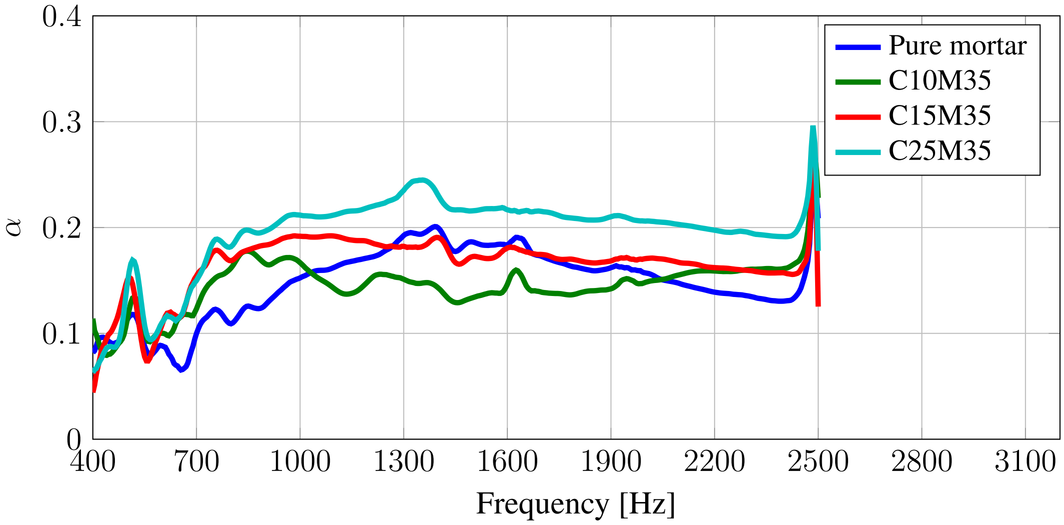

(b) Absorption coefficient for 35 mesh composites

Figure 4.1: Absorption coefficient for mortar/rubber composites as a function of composition and rubber particle granulometry

that can be relatively heavy (e.g., use of an anechoic termination or two different terminations, up to four microphones and six transfer function measurements);

3. The inverse methods, based on an optimization problem where the properties are adjusted in the model to reproduce acoustic measurements, generally uses a surface acoustic property to operate (e.g., sound absorption coefficient or surface impedance).

An optimization method was applied in this work in order to determine the macroscopic JCA parameters. According to Atalla and Panneton, porosity and air flow resistivity can be experimentally determined using standard techniques, remaining a vector of three unknown parameters: the tortuosity α_∞, the viscous characteristic length Λ and the thermal characteristic length Λ' (Atalla and Panneton, 2005). Nevertheless, air flow resistivity was not measured in this work, thus the unknown parameter are $\alpha_\infty, \sigma, \Lambda, \Lambda'$. As the porosity value measured by X-ray microtomography and depicted in Chapter 2 was based on a $2\times2\times2$ mm heterogeneous sample, this parameter was also included into the optimization variables in order to have an adjusted curve using the JCA model.

Curves shown in Figure 4.1 were adjusted by the JCA model by least squares method. Figure 4.2 presents the experimental and adjusted curves of sound absorption coefficient as a function of frequency for pure mortar and mortar/rubber composites. In order to promote a satisfactory adjustment, the frequency range was chosen to be from 575 Hz to 2400 Hz, avoiding the frequency regions in which the experimental curves presented lower coherence values. The porosity values estimated by X-ray microtomography were used as initial values for the least squares adjustment. The other starting values for the flow resistivity, tortuosity, thermal and viscous characteristics lengths are 7E5 Ns/m^4, 1 (for the pure mortar) and 3 (for the other samples), 1.5E-6 m, and 80E-6 m respectively. Table 4.1 shows the values of porosity, tortuosity, flow resistivity (R), thermal (Λ') and viscous (Λ) characteristics lengths obtained from JCA model curve fitting to experimental data. For comparison, the porosity values obtained by X-ray microtomography are presented in parenthesis. These adjustments were performed using the function *lsqcurvefit* of MATLAB software, which solves a non-linear least squares problem returning the parameters which best approximate the objective function output to the experimental data. The termination tolerance for the function value was 1E-16 and the termination tolerance for the point variation was 1E-8. Upper and lower parameters limits were also established having coefficients ranges from 0 to 1 for porosity, 1 to 20 for tortuosity and 0 to 1E8 for flow resistivity. Limits for viscous and thermal lengths from 0 to 0.0052 were used for pure mortar and for C10M35 and C15M35 samples, from 0 to 0.0051 for C10M60 sample, from 0 to 0.0056 for C15M60 sample, from 0 to 0.00555 for C25M60 sample and from 0 to 0.0058 for C25M35 sample.

Table 4.1: JCA model curve fitting to experimental data - absorption coefficient (X-ray microtomography values of porosity in parenthesis)

Sample	Porosity [%]	Tortuosity	σ [Nsm^{-4}]	Λ [m]	Λ' [m]
mortar	43.1 (25.4±0.8)	1.5	6.3E5	7.3E-7	2.1E-4
C10M60	47.2 (45.0±0.9)	2.5	3000	4.6E-7	6.4E-5
C15M60	60.5 (57.0±1.0)	2.2	1.8E6	6.6E-7	1.0E-4
C25M60	82.4 (66.4±0.5)	2.7	1.0E6	2.8E-6	2.5E-4
C10M35	59.5 (44.2±0.9)	2.0	2.8E6	1.2E-6	1.9E-4
C15M35	57.5 (45.8±0.3)	3.0	1.8E6	1.3E-6	1.1E-4
C25M35	62.7 (60.3±0.4)	3.0	1.6E6	1.5E-6	1.3E-4

It is possible to note that the porosity values obtained by fitting the experimental data to the JCA model are always higher than those obtained by X-ray microtomography, however, in the case of C15M60 and C25M35 samples, the obtained porosity by both techniques are relatively close. This model is based on porous materials with interconnected pores forming channels and a smooth variation of the cross section. As seen in Figure 2.3 (h), the voids observed in pure mortar has no regular shape, and size and this could explain the differences between the values of porosity obtained in the X-ray microtomography and by the JCA model based on the measured α in the impedance tube. Another factor that could be related to the porosity difference is the dimension of the analyzed specimen due to the heterogeneous nature of the samples. For X-ray microtomography experiments, samples were reducted from 60 mm in diameter to pieces of approximately 2×2×2 mm to enable correct placement into the microtomography equipment, otherwise the entire sample was analyzed in the impedance tube. It is possible that in the X-ray microtomography, the specimen size was not large enough to represent the sample

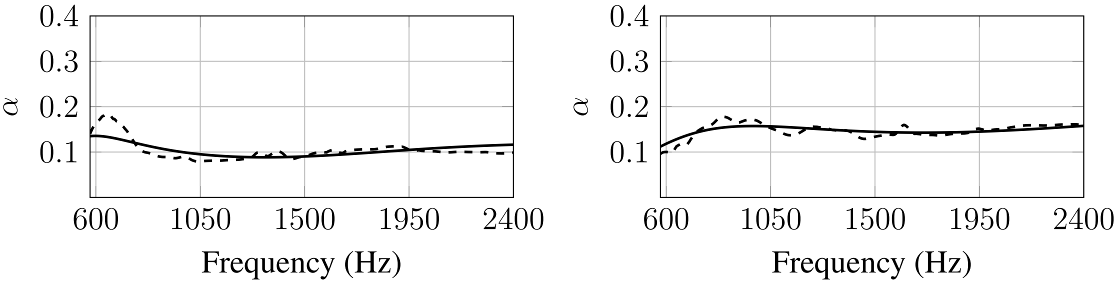

(a) C10M60 (b) C10M35

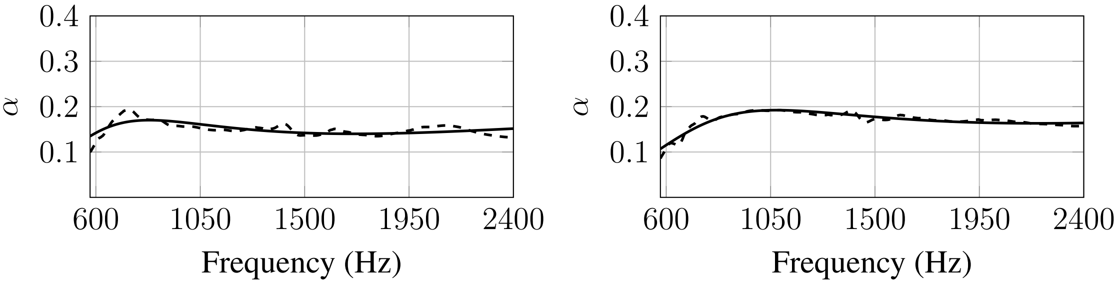

(c) C15M60 (d) C15M35

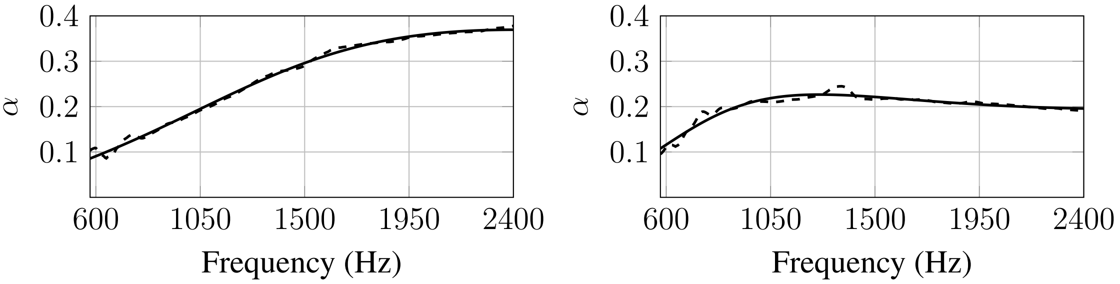

(e) C25M60 (f) C25M35

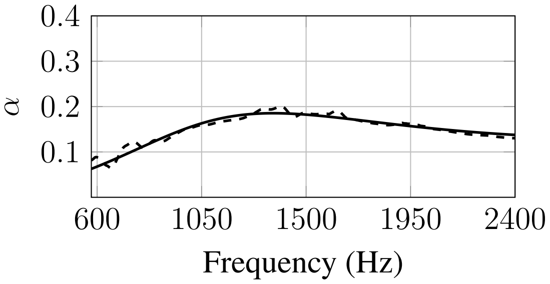

(g) Pure mortar

—— JCA model – – – Experimental

Figure 4.2: JCA model adjustment to experimental data of the samples

as a whole for a good porosity estimation. Besides this, JCA model led to a satisfactory fit.

Observing the experimental curves of absorption coefficient in the frequency and comparing the results of the composites with the results of the pure mortar, it can be noted that the C25M60 presented the highest α across the frequency band, followed by the C25M35. These samples also showed higher porosity values, C25M60 is more porous than C25M35, both for X-ray microtomography and JCA model estimate.

From Table 4.1, it is possible to note that the samples C10M35, C15M35 and C15M60 presented very close porosity values to the sample C25M35. If α was influenced only by this factor, it would be expected that C10M35, C15M35 and C15M60 values of α would be also greater than those observed for pure mortar in the analyzed frequency range. But this was not observed. Moreover, if the curves of α for samples C25M60 and C25M35 are compared, it can be noted that values of α for sample C25M35 are higher than those of the sample C25M60 until the frequency near 1150 Hz, and from this frequency on, the α becomes higher for the sample C25M60. These behaviors suggest the need to consider the influence of additional parameters in the sound absorption besides the porosity.

Analyzing the curves of samples prepared with M60 rubber, one can notice that both C10M60 and C15M60 exhibit high absorption in the low frequency region and maximum α occurred at 650 Hz and 740 Hz respectively. Considering the pure mortar curve as reference, it is verified that the sample C10M60 presents higher α until approximately 760 Hz, and after this frequency, α is always smaller. The values of α of sample C15M60 are higher until about 1020 Hz compared to pure mortar, α becomes lower until near 2000 Hz, and from this frequency on, the curves practically overlap. The pure mortar curve shows maximum values of α in a wider frequency range between 1350 Hz and 1600 Hz.

For samples prepared with M35 rubber, one can notice that the sample C10M35 presents a very similar behavior to the C15M60, with maximum α in the range from 750 Hz to 800 Hz. The sample C15M35, compared to the pure mortar, has higher α in two frequency ranges (from

550 Hz to 1250 Hz and above 2000 Hz). In the range from 1250 Hz to 2000 Hz, the values of α for C15M35 are close to those of the pure mortar.

Samples were separated in two groups to analyze the effect of the flow resistivity according to values of α considering the pure mortar as reference. In the first group, samples C25M60 and C25M35 are analyzed because they presented higher α than the pure mortar for all frequency range. The other samples are considered in the second group. As shown in Table 4.1, it is possible to verify that the flow resistivity of the sample C25M60 is lower than for the sample C25M35, suggesting that in the low frequency region, the α values of the sample C25M60 should be smaller than for the C25M35. In the high frequency region, the opposite should occur. This was verified in the experimental curves of α. Higher values of α were observed for the sample with lower flow resistivity from frequency over approximately 1150 Hz.

For the other samples, the analysis of the flow resistivity has been restricted to low frequency region, where the influence of this parameter appears to be greater. The values of α for samples C10M60, C15M60, C10M35 and C15M35 were higher than the pure mortar until certain frequency values (as described above, near to 760 Hz, 1020 Hz, 1020 Hz and 1250 Hz, respectively). The estimated flow resistivity values for composites C15M60, C10M35 and C15M35 are higher than the pure mortar, which suggests that at low frequency, the composites would show higher α compared to the pure mortar as indeed it was observed. The estimated value of flow resistivity for the sample C10M60 was several orders of magnitude smaller than the estimated value for the other samples suggesting that this composite presents the smallest α compared to all samples in low frequency region. This was not observed probably due to the shift of absorption maximum to lower frequencies due to tortuosity increasing as shown in Table 4.1. Note that the estimated tortuosity values for the composites are higher compared to pure mortar, whose estimated value was 1.5. For the sample C10M60, the estimated tortuosity is 2.5, which is in agreement to the shift of the maximum absorption at lower frequencies.

4.2 Transmission Loss

Transmission loss results, as well as the absorption ones, were obtained by considering the mean value of each sample's replicas. Figure 4.3 shows the TL variation as a function of frequency, for pure mortar and mortar/rubber composites. For all samples, it can be seen that TL curves present some depressions and elevations. TL maximum values for almost all the samples occurred in two frequency ranges (near 700 Hz to 750 Hz, and near 1800 Hz to 2200 Hz), and the TL minimum values occurred in frequency values near to 1000 Hz, except for C10M35. For this composite, a minimum TL value appeared near 600 Hz, and the maximum occurred in the frequency range from 1100 Hz to 1800 Hz. For this particular sample, it was also observed a sudden TL drop near to 2200 Hz.

As detailed in Section 3, first resonance frequency can be estimated by Equation (3.26) and it is required to know the Young's Modulus which was obtained by compressive test for pure mortar. Seven samples with 20.98±0.33 mm diameter and 54.73±6.25 mm height were prepared. Figure 4.4 shows the obtained stress versus stain graphic. A linear regression was made in order to obtain the slope and thus the Young's Modulus E.

Table 4.2 shows the obtained elasticity modulus for pure mortar samples, and the mean obtained modulus is 492.61±240.76 MPa. For the first resonance frequency it was considered: $D = 60$ mm, $h = 5$ mm and $\rho = 1500$ kg/m^3. The Poisson's ratio was considered as 0.15 according to reported values of mortars for structural masonry (Campello, 2013; Mohamad et al., 2009). So, for pure mortar, f_{r1} could be between 789 Hz and 1960 Hz, considering the minimum and maximum values of the Young's Modulus.

The first minimum value of TL was verified at 1050 Hz. TL curve for pure mortar can be analyzed considering the regions before and after 1050 Hz. For frequencies below 1050 Hz, it is considered the stiffness controlled region, and after this frequency the resonance troughs start allowing to consider f_{r1} = 1050 Hz.

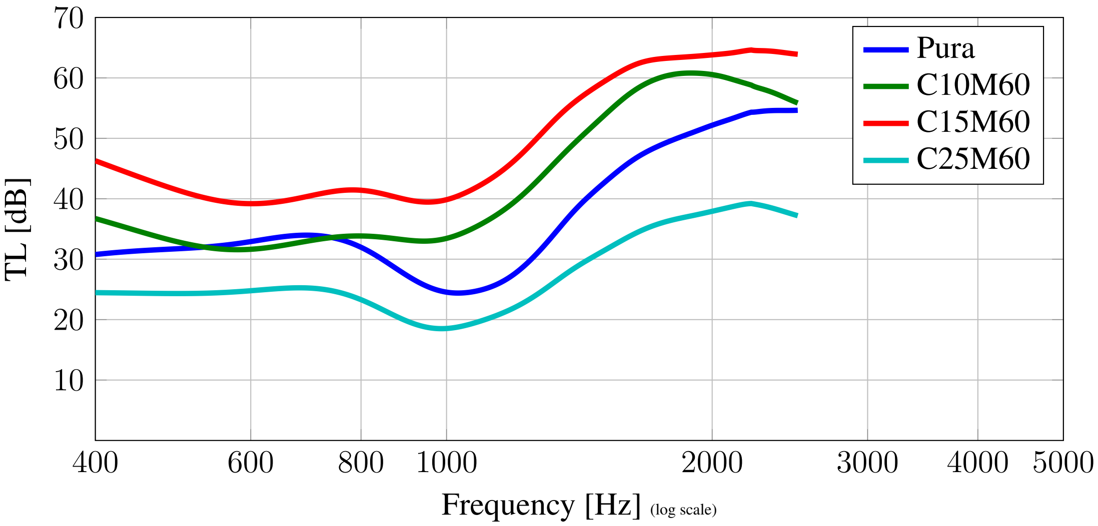

(a) TL variation for M60 composites

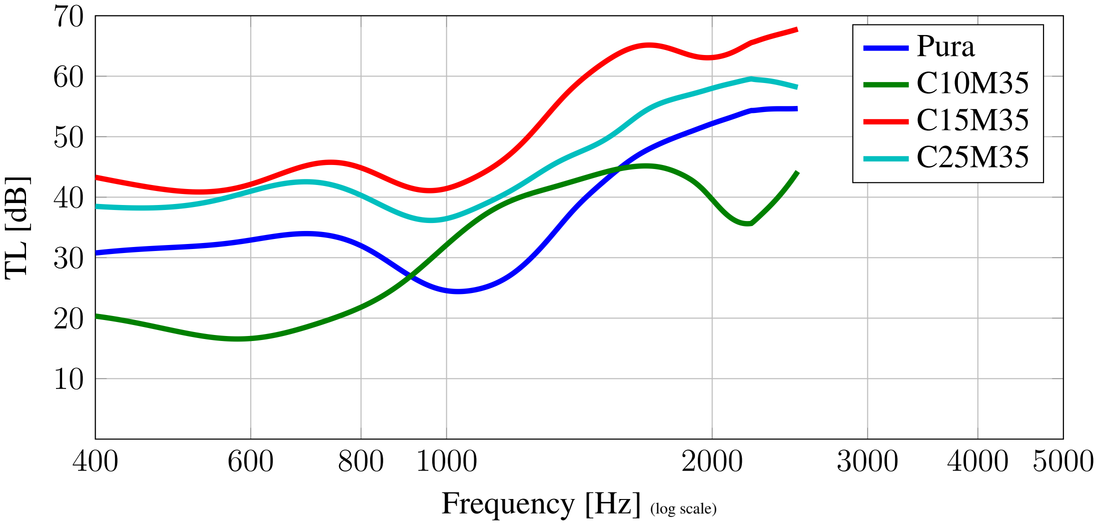

(b) TL variation for M35 composites

Figure 4.3: Transmission Loss for mortar/rubber composites as a function of composition and rubber particle granulometry

Table 4.2: Young's Modulus for pure mortar samples

Sample	Diameter [mm]	height [mm]	E [MPa]
1	21.0	58.7	774.64
2	21.5	57.6	379.94
3	21.0	48.2	279.33
4	20.6	43.5	126.03
5	21.3	58.8	743.44
6	20.6	57.1	576.01
7	20.9	59.2	568.89
Average	20.99	54.73	492.61
Standard deviation	0.33	6.25	240.76

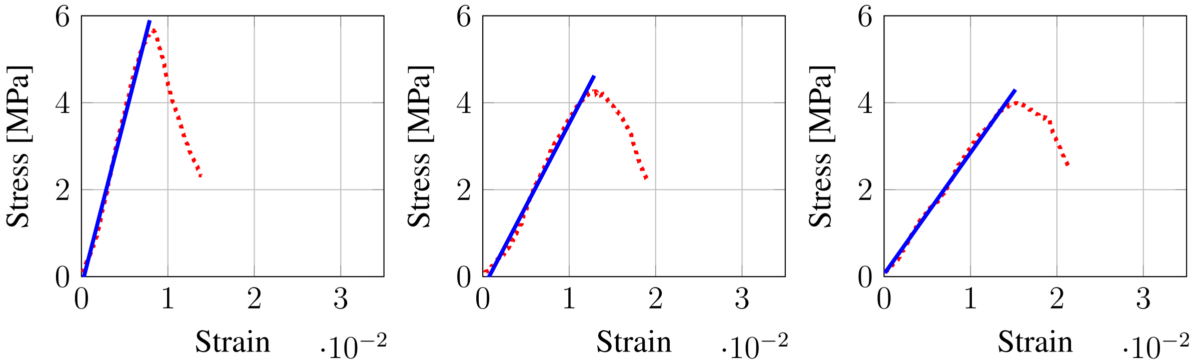

(a) Pure mortar sample 1 (b) Pure mortar sample 2 (c) Pure mortar sample 3

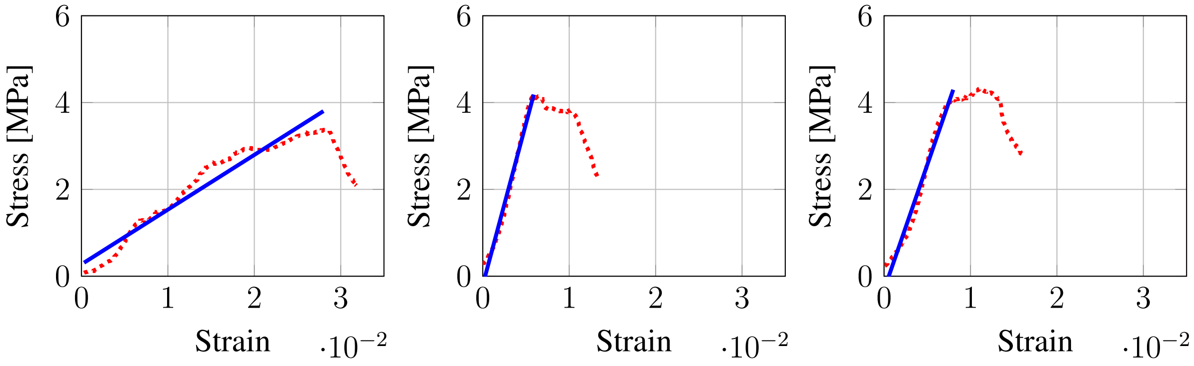

(d) Pure mortar sample 4 (e) Pure mortar sample 5 (f) Pure mortar sample 6

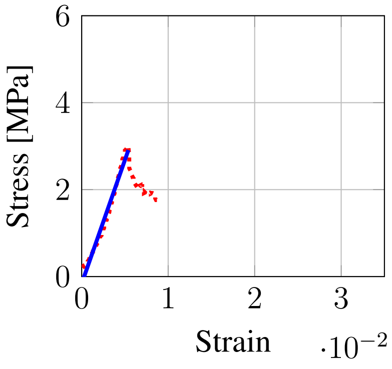

(g) Pure mortar sample 7

Figure 4.4: Stress versus Strain plots for pure mortar samples

4.3 TL prediction

It was compared the experimental curve with the curve obtained from the TMTX software, assuming a single layer system surrounded by air. To calculate the system TL, the program uses some material properties, i.e., density, Young's modulus and Poisson's ratio for solid materials (Tanneau et al., 2006). For pure mortar sample it was used the average Young's modulus obtained in the compression test $E = 492.61$ MPa, ρ = 1510 kg/m^3, ν = 0.15 and $h = 5$ mm. Comparing the experimental curve obtained for the pure mortar with the model curve shown in Figure 4.5 (a), one can note that the experimental curve does not follow a specific behavior, indicating that the mathematical treatment used to describe sound transmission behavior by homogeneous solid panels can not be used in this case.

Nevertheless, it is interesting to note that the composites C15M60 and C15M35 presented higher values of TL compared to the pure mortar throughout the analyzed frequency range. Despite knowing that mortar composites are heterogeneous materials, it was used the same TMTX model to obtain the theoretical TL for those composites; models for heterogeneous porous materials use some mechanical properties other than the mentioned above for JCA model as the damping coefficient, Young's modulus and Poisson's ratio, which were not obtained in this work. For this modeling, Young's modulus was fixed at the same value than pure mortar and ν = 0.44 was calculated by using TL = 45.78 dB at 400 Hz for C15M60 sample and ν = 0.45 for TL = 42.35 dB at 400 Hz. It was chosen the lowest measured frequency value because ν needs to be calculated in the stiffness controlled region and, assuming a similitude between pure mortar and composites, f_{r1} for composites is probably located below 789 Hz. Those approximations are shown in Figure 4.5 (b) and 4.5 (c). Note that ν for pure mortar was established at 0.15 as it appears in literature and calculated for composites due to the Poisson's coefficient for composites was not available in literature.

Sgard and Atalla (Sgard and Atalla, 2000) investigated the TL modeling as function of the frequency of a heterogeneous porous material consisting on a porous material containing

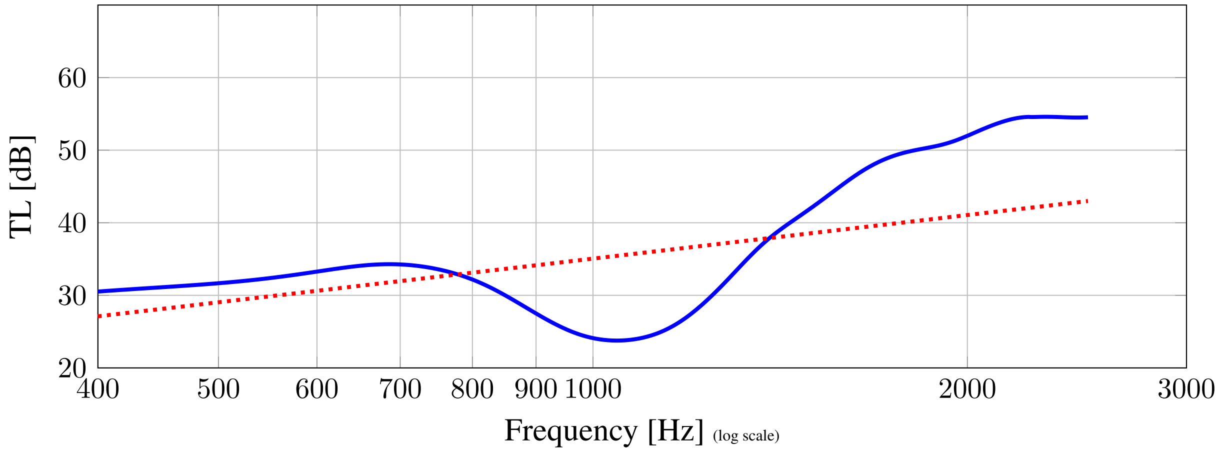

(a) Pure sample

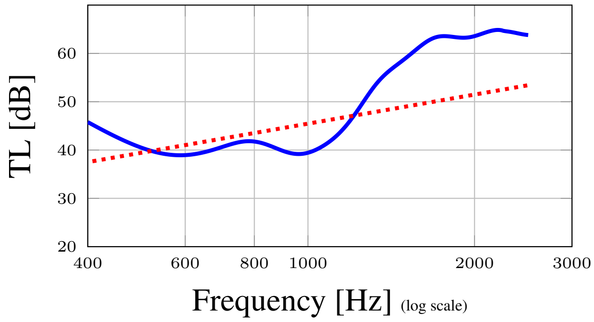

(b) C15M60 sample

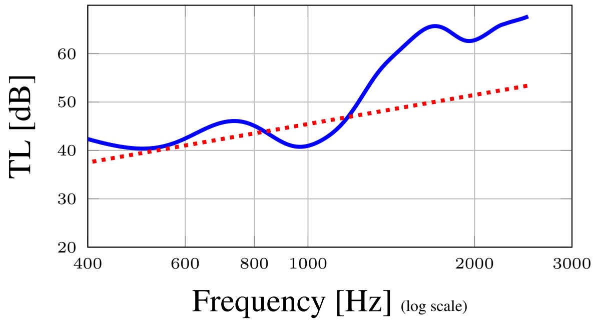

(c) C15M35 sample

Figure 4.5: Comparison between experimental and theoretical TL calculated with the estimated mechanical properties properties

particles of a solid material with lower density than the density of the porous material. In this reference, a square panel with 10 cm side and 3.75 cm thickness was considered. The TL was not affected by the presence of solid particles in the low frequency region. But in the high frequency region, the TL of the heterogeneous material was greater than that of the porous material without the solid particles.

The effect of the heterogeneity of the material in the acoustic properties has been a concern in several studies, especially considering double porosity materials. In these cases, investigations are more focused on sound absorption (Sgard et al., 2000; Olny and Boutin, 2003; Bécot et al., 2011; Atalla et al., 2001; Castillo, 2011; Xiao et al., 2012). It is intended in a future work, to analyze TL results for both pure mortar and for mortar/rubber composites through a model that considers the effects of heterogeneity and porosity of the material.

In order to know the samples behavior in a floor system, it was simulated a three layer system with finishing, fixation and structural layer. It was also employed the TMTX software (Tanneau et al., 2006). The system was composed by five layers as shown in Figure 4.6. Layers 1 and 5 are the fluid surrounding the system, in this case, air.

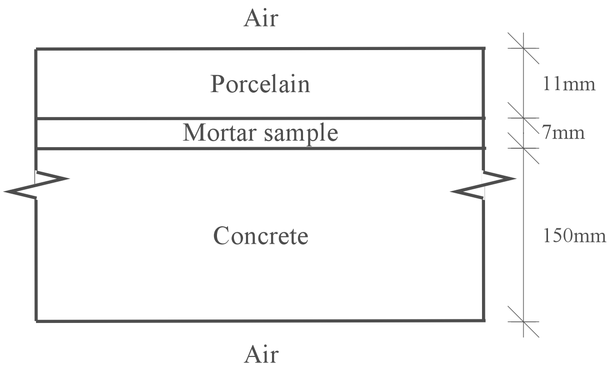

Figure 4.6: Floor system employed for the TMTX simulation

Then, the materials properties of each layer were added on the TMTX, porcelain for the finishing layer, pure mortar and composites in the fixation layer and concrete in the structural layer. Mechanical properties for concrete, porcelain and air are shown in Table 4.3.

Figure 4.7 shows the obtained results for a floor system changing the third layer mate-

Table 4.3: Mechanical properties for Porcelain and Concrete

	E [GPa]	ν	$\rho\,[\frac{Kg}{m^3}]$	$c\,[\frac{m}{s}]$
Porcelain	60	0.25	2200	–
Concrete	2.07	0.13	2400	–
Air	–	–	1.3	342

rial. System was exposed to a simple incidence wave at 0° in order to be consistent with the experimental test on the impedance tube. As expected, transmission loss increases with the addition of the flooring and the concrete layer. Exposed to the same conditions, floor systems with C15M35 and C15M60 composites presented a higher TL than the floor system with the pure mortar. However, TL did not present variations from sample with 60 mesh and 35 mesh below 1400 Hz. This behavior can be due to the mass influence in the TL region, in this case, apparent density was 1110 kg/m^3 and 1150 kg/m^3 for C15M60 and C15M35 composites respectively.

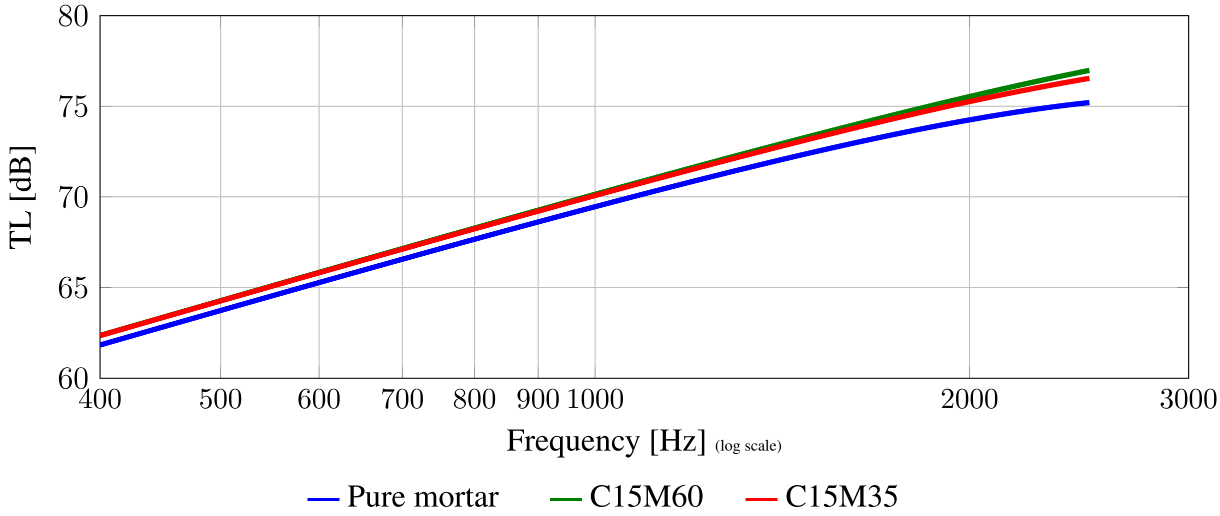

Figure 4.7: TL for simulated floor system with each sample

4.4 Tensile Bond Strength

In order to know the variation on the mechanical properties of the mortar with the rubber addition, tensile bond strength tests were performed for mortar/rubber composites containing 15% of rubber particles, since these samples showed best TL results in all the investigated frequency range. Tests were also performed for pure mortar in order to compare the results.

In tensile bond strength tests, once the force is applied, five kinds of separation can occur as seen in Figure 4.8:

1. Substrate rupture (S), which is a breaking in the substrate.
2. Mortar/Substrate interface rupture (SM), which is a breaking or separation between mortar and substrate.
3. Mortar rupture (M), which indicates a breaking in the mortar.
4. Mortar/Ceramic-Plate interface rupture (MP), which is a breaking or separation between mortar and ceramic plate.
5. Ceramic-Plate rupture (P), which is the ceramic plate breaking.

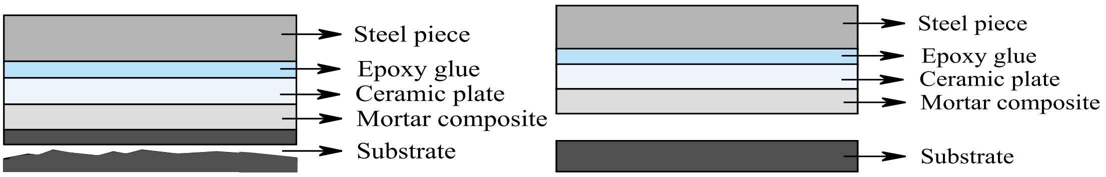

(a) Substrate rupture (S)

(b) Mortar/substrate interface rupture (S/M)

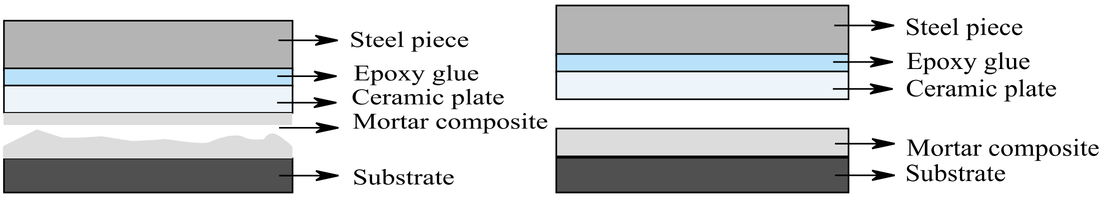

(c) Mortar rupture (M)

(d) Mortar/ceramic plate interface rupture (M/P)

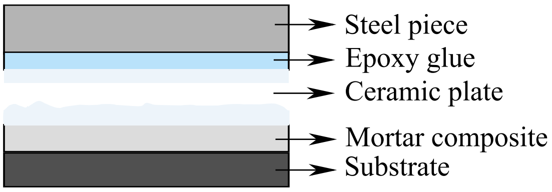

(e) Ceramic plate rupture (P)

Figure 4.8: Tensile bond strength test separation types

Results for pure mortar are shown in Table 4.4. It is possible to find more than one kind of rupture on a block and they are measured in percentage proportions. Results for block number 5 were discarded due to a premature separation of the ceramic plate and the mortar caused by an irregularity on the mortar application observed at the left of block 5 as shown in Figure 4.9 (a).

Table 4.4: Tensile bond strength results for Pure mortar

Block	Kind of rupture					Force [kN]	Breaking stress [MPa]
	S	S/M	M	M/P	P		
1			100%			0.34	0.14
2			95%	5%		0.20	0.08
3			100%			0.70	0.28
4			95%	5%		0.20	0.08
5	-	-	-	-		-	-
6			90%	10%		0.31	0.12
7			70%	30%		0.63	0.25
8			100%			0.87	0.35
9			90%	10%		0.36	0.14
10			100%			0.67	0.27
Average						0.48	0.19
Standard deviation						0.24	0.10

C15M60 sample results are shown on Table 4.5. In this case, plates 6, 8 and 10 presented a premature separation and were discarded. Figure 4.9 (b) shows a mortar application irregularity on those blocks.

Table 4.5: Tensile bond strength results for C15M60 mortar/rubber composite

Block	Kind of rupture					Force [kN]	Breaking stress [MPa]
	S	S/M	M	M/P	P		
1			100%			0.18	0.07
2			95%	5%		0.15	0.06
3			100%			0.18	0.07
4			100%			0.22	0.09
5			100%			0.17	0.07
6	-	-	-	-	-	-	-
7			100%			0.09	0.04
8			100%			0.12	0.05
9	-	-	-	-	-	-	-
10	-	-	-	-	-	-	-
Average						0.16	0.06
Standard deviation						0.04	0.02

For sample C15M35, results are shown on Table 4.6.

The breaking stress average for each sample was computed and presented on Tables 4.4,

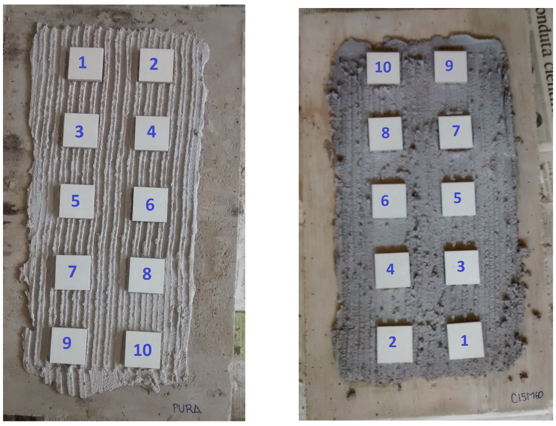

(a) Pure sample (b) C15M60 composite

Figure 4.9: Mortar layer irregularities for Pure mortar and C15M60 composite

Table 4.6: Tensile bond strength results for C15M35 mortar/rubber composite

Block	Kind of rupture					Force [kN]	Breaking stress [MPa]
	S	S/M	M	M/P	P		
1		100%				0.08	0.03
2				100%		0.11	0.04
3			80%	20%		0.24	0.10
4			85%	15%		0.15	0.06
5			100%			0.18	0.07
6			100%			0.10	0.04
7			90%	10%		0.16	0.06
8			100%			0.17	0.07
9			100%			0.14	0.06
10			100%			0.14	0.06
Average						0.15	0.06
Standard deviation						0.05	0.02

4.5 and 4.6 showing a reduction of adherence for the composites when compared with the pure mortar.

Nevertheless, considering the standard deviation, it is possible to see that minimum value of breaking stress on Pure mortar [0.08 MPa] is quite close with maximum breaking stress values on C15M60 [0.09 MPa] and C15M35 [0.10 MPa] samples.

Concerning the low breaking stress values, the pure mortar tested here presented lower values compared to expected values from ABNT 14081 (ABNT 14081, 2004), which specifies a breaking stress of 0.5 MPa. The same water quantity (200 ml) and the same mixing time (30 seconds) were used for pure mortar and composite preparation. Some uncertainties arise due to variation on relative humidity and curing temperature. As all the samples were submitted to the same conditions, we believe that these uncertainties affected in the same form the obtained results.

5 Conclutions

The aim of this work was to reuse rubber particles from discarded tires trough the preparation of a composite material made with different levels of rubber particles and mortar to verify the potential of reducing the airborne noise coming from upstairs to downstairs in buildings.

A factorial experiment considering two factors that affect the response, composition and granulometry was designed, with 3 and 2 levels respectively. 14 samples were prepared and their absorption coefficient and transmission loss were experimentally evaluated.

Compared to pure mortar, mortar/rubber composites containing 10, 15 or 25$\%$ of rubber particles with granulometries between 18 and 35 mesh and between 35 and 60 mesh showed lower density values. Phase separation was not observed in scanning electron microscopy, but X-ray microtomography analysis clearly showed the presence of domains with different densities. By using the X-ray microtomography, it was also possible to estimate the porosity of pure mortar and mortar/rubber composites.

Sound absorption behavior was evaluated by considering the variation of the sound absorption coefficient (α) in the frequency range from 400 Hz to 2500 Hz. Composites containing 25$\%$ of rubber particles showed the highest values of sound absorption coefficient in all investigated frequency range. The experimental curves of α versus frequency were fitted to Johnson-Champoux-Allard model showing that sound absorption behavior mainly depended on porosity.

Samples with the higher transmission loss are the better, since they have a better airborne noise insulation. Samples C15M60 and C15M35 presented the higher TL values with an intermediate α. In future work, it is intended to analyze the transmission loss behavior for both pure mortar and mortar/rubber composites using models that consider the effects of heterogeneity and porosity of the acoustic panels, for example, the model developed by Sgard and Atalla (Sgard and Atalla, 2000; Sgard et al., 2000; Atalla et al., 2001), as well as the evaluation of impact noise insulation potential.

For frequencies from 500 Hz to 600 Hz, samples C10M35, C15M60, C15M35 and C25M35 have a similar TL, which means that for those frequencies, changes in composition do not make a big difference on insulation. It is necessary to consider some uncertainties in the analysis such as the variations preparation process, the noise present in the signal due to the measurement process, and the pores distribution of the samples. The simulated floor system presented similar results for composites. The samples C15M60 and C15M35 presented the best insulation behavior in this case.

Results on Section 4.4 evidence that even though a decrease in the adhesion strength occurred, a composite of 85$\%$ mortar and 15$\%$ rubber could be employed in constructions in order to contribute on noise insulation. Perhaps, as shown in previous works, mechanical properties of rubberized cementitious materials can be improved by adding another aggregate as silica fume or previously treating the rubber in order to improve the rubber interaction with the mortar matrix (Elchalakami, 2014; Segre and Joekes, 2000; Raghavan, 2000).

For tests replication, a chemical characterization of the rubber particles was made in order to have an accurate idea of its composition. M35 and M60 rubber contain natural rubber mixed with Styrene-butadiene rubber (SBR) or polybutadiene rubber (BR), or mixed with both SBR and BR.

For future work, it is important to determine the air flow resistivity in order to determine the JCA parameters based on porosity and flow resistivity. Elasticity modulus and the Poisson's ratio for composites should be determined in order to compare theoretical results with experimental ones, and first resonance frequency can also be experimentally measured. It is also interesting to deeply study the C25M60 absorption coefficient since it showed a different behavior compared to other composites and the pure mortar.

References

ABNT 14081, 2004. Argamassa colante industrializada para assentamento de placas cerâmicas - requisitos.

ABNT 14082, 2004. Argamassa colante industrializada para assentamento de placas cerâmicas. Execução do substrato-padrão e aplicação de argamassa para ensaios.

ABNT 14084, 2004. Argamassa colante industrializada para assentamento de placas cerâmicas. Determinação da resistência de aderência à tração.

ABNT 15575, 2013. Edificações habitacionais - desempenho. Parte 3: Requisitos para os sistemas de pisos.

Almeida Júnior, A. F., Battistelle, R. A., Bezerra, B. S., de Castro, R., 2012. Use of scrap tire rubber in place of SBS in modified asphalt as an environmentally correct alternative for Brazil. Journal of Cleaner Production 33, 236–238.

ANIP, 2015. Livro branco da indústria de pneus - uma política social para o setor. Tech. rep., ANIP, São Paulo, SP.

APMR, Accessed: April 2016. Johnson-Champoux-Allard (JCA) model. http://apmr.matelys.com/PropagationModels/MotionlessSkeleton/ JohnsonChampouxAllardModel.html.

Atalla, N., Panneton, R., Sgard, F., Olny, X., 2001. Acoustic Absorption of Macro-Perforated

Porous Materials. Journal of Sound and Vibration 243 (4), 659–678.

Atalla, Y., Panneton, R., 2005. Research article/Article de recherche. Canadian Acoustics 33 (1), 11–24.

Aubicon, Accessed: November 2015. Sound soft mantas acústicas. http://www.aubicon.com.br/produtos/mantas-acusticas-sound-soft.html.

Barron, R. F., 2001. Industrial Noise Control and Acoustics. Marcel Dekker, Inc.

Bécot, F. X., Jaouen, L., Sgard, F., 2011. Noise control strategies using composite porous materials - Simulations and experimental validations on plate/cavity systems. Noise Control Eng. J 59 (5), 464–475.

Bolton, J. S., Yoo, T., Olivieri, O., 2007. Measurement of normal incidence transmission loss and other acoustic properties of materials placed in standing wave tube. Tech. rep., Brüel & Kjaer.

BSWA Tech, 2010. BSWA TECH. User's Manual - Impedance Tube Tests System.

Campello, E. F., 2013. Comportamento mecânico de argamassas reforçadas por fibras sintéticas e metálicas. Ph.D. thesis, Universidade Federal Fluminense, Rio de Janeiro - RJ, Brazil.

Canova, J. A., Bergamasco, R., Angelis Neto, G. D., 2008. A utilização de resíduos de pneus inservíveis em argamassa de revestimento. Acta Scientiarum. Technology 29 (2), 141–149.

Castillo, R. G. V., 2011. Microstructure influence on acoustical properties of multi-scale porous materials. Ph.D. thesis, University of Salford, Manchester, U.K.

CEMPRE, Accessed: March 2016. Pneus. http://cempre.org.br/artigo-publicacao/ficha-tecnica/id/7/pneus.

Champoux, Y., Allard, J.-F., 1991. Dynamic tortuosity and bulk modulus in air-saturated porous media. Journal of Applied Physics 70 (4), 1975–1979.

CONAMA, 2012. Resolution 416/2009 of the national environmental council. Tech. rep.

Costa, M., Cincotto, M. A., Pileggi, R., 2005. Análise comparativa de argamassas colantes de mercado e o seu comportamento reológico. In: VI Simpósio Brasileiro de Tecnologia de Argamassas.

Cox, T., D'Antonio, P., 2006. Acoustic Absorbers and Diffusers, Theory, Design and Application. Spon Press, New York.

Dall'Antonia, A. C., Martins, M. A., Moreno, R. M., Mattoso, L. H., Gonçalves, P. S., Job, A. E., 2009. Caracterização mecânica e térmica da borracha natural formulada e vulcanizada dos clones: GT 1, IAN 873, PB 235 e RRIM 600. Polímeros: Ciência e Tecnologia 19 (1), 63–71.

Doutres, O., Salissou, Y., Atalla, N., Panneton, R., 2010. Evaluation of the acoustic and non-acoustic properties of sound absorbing materials using a three-microphone impedance tube. Applied Acoustics 71 (6), 506–509.

Elchalakami, M., 2014. High strength rubber concrete containing silica fume for the construction of sustainable road side barriers. Structures (1), 20–38.

Galiani, P. D., 2010. Avaliação e caracterização da borracha natural de diferentes clones de seringueira cultivados nos estados de mato grosso e bahia. Ph.D. thesis, Universidade Federal de São Carlos, São Carlos - SP, Brazil.

Gerges, S., 2000. Ruído: Fundamentos e controle, 2nd Edition. NR Editora, Consultoria e Treinamento, Florianopolis, Brazil.

Halasa, A. F., Massie, J., 2000. Polybutadiene. John Wiley & Sons.

Holmes, N., Browne, A., Montague, C., 2014. Acoustic properties of concrete panels with crumb rubber as a fine aggregate replacement. Construction and Building Materials (73), 195–204.

Honorato, A. M. B., 2013. Avaliação de modelos analíticos para a determinação de absorção sonora de materiais poroelásticos. Master's thesis, Universidade Federal de Santa Catarina, Florianópolis - SC, Brazil.

Isaia, G. C., 2007. Materiais de construção civil e princípios de ciência e engenharia de materiais. IBRACON, São Paulo, SP.

ISO 10534-2, 2001. Acoustics. determination of sound absorption coefficient and impedance in impedance tubes. Part 2: Transfer-function method.

Johnson, D. L., Koplik, J., Dashen, R., 1987. Theory of dynamic permeability and tortuosity in fluid-saturated porous media. Journal of Fluid Mechanics 176 (1), 379.

Jung, S. S., Kim, Y. T., Lee, Y. B., Cho, S. I., Lee, J. K., 2008. Measurement of Sound Transmission Loss by Using Impedance Tubes. Journal of the Korean Physical Society 53 (2), 596.

Khan, A., 2008. Vibro-acoustic products from re-cycled raw materials using a cold extrusion process: a continuous cold extrusion process has been developed to tailor a porous structure from polymeric waste, so that the final material possesses particular vibro-acoustic . Ph.D. thesis, University of Bradford.

Litvin, A., Belliston, H. W., 1978. Sound transmission loss through concrete and concrete masonry walls. Journal of the American Concrete Institute 75 (12), 2–10.

Mafra, M. P., Soeiro, N. S., Alves, E., 2005. Determinação e análise comparativa dos coeficientes de absorção de paineis confeccionados a partir da fibra de coco e um painel de uso comercial. In: XII Congresso Nacional de Estudantes de Engenharia Mecânica.

Mareze, P. H., 2013. Análise da influência da microgeometria na absorção sonora de materiais porosos de estrutura rígida. Ph.D. thesis, Universidade Federal de Santa Catarina, Florianópolis - SC, Brazil.

Mohamad, G., Neto, A. S., Pelisser, F., Lourenço, P., Roman, H., 2009. Caracterização mecânica das argamassas de assentamento para alvenaria estrutural - previsão e modo de ruptura. Matéria (Rio de Janeiro) 14 (2), 824–844.

Mohammed, B. S., Anwar Hossain, K. M., Eng Swee, J. T., Wong, G., Abdullahi, M., 2012. Properties of crumb rubber hollow concrete block. Journal of Cleaner Production 23 (1), 57–67.

Munjal, M., 2013. Noise and Vibration Control. IISc lecture notes series. World Scientific Publishing Company, Singapore.

Nallasamy, P., Anbarasan, P., Mohan, S., 2002. Vibrational spectra and assignments of cis- and trans-1.4-polybutadiene. Turk J Chen 26, 105–111.

Norton, M., Karczub, D., 2003. Fundamentals of Noise and Vibration Analysis for Engineers.

Cambridge University Press.

Olny, X., Boutin, C., 2003. Acoustic wave propagation in double porosity media. The Journal of the Acoustical Society of America 114 (1), 73.

Paixão, D. X., 2002. Caracterização do isolamento acústico de uma parede de alvenaria, utilizando análise estatística de energia. Ph.D. thesis, Universidade Federal de Santa Catarina, Florianópolis - SC, Brazil.

Pfeifer, W. P., 2012. Electromagnetic characteristics of cement paste and waste rubber. Master's thesis, University of Campinas, Campinas - SP, Brazil.

Raghavan, D., 2000. Study of rubber-filled cementitious composites. Journal of Applied Polymer Science 77 (4), 934–942.

Rocha, T. L., Schuster, R. H., Jacobi, M. M., Samios, D., 2004. Estudo da modificação química de polidienos do tipo sbr e br. Polímeros: Ciência e Tenología 14 (5), 318–321.

Segre, N., Joekes, I., 2000. Use of tire rubber particles as addition to cement paste. Cement and Concrete Research 30 (9), 1421–1425.

Serrano, C. L. R., 2009. Uso de resíduo de sbr proveniente sa indústria de cançados em composições de sbr. Ph.D. thesis, Universidade Federal do Rio Grande do Sul, Porto Alegre - RS, Brazil.

Sgard, F. C., Atalla, N., 2000. Transmission loss through barriers lined with heterogeneous porous materials. In: Canadian Acoustics. Vol. 28. pp. 92–93.

Sgard, F. C., Atalla, N., Nicolas, J., 2000. A numerical model for the low frequency diffuse field sound transmission loss of double-wall sound barriers with elastic porous linings. The Journal of the Acoustical Society of America 108 (6), 2865–2872.

Struik, L., 1987. The mechanical behaviour and physical ageing of semicrystalline polymers: 2. Polymer 28, 1534–1542.

Su, H., Yang, J., Ling, T.-C., Ghataora, G. S., Dirar, S., 2015. Properties of concrete prepared with waste tyre rubber particles of uniform and varying sizes. Journal of Cleaner Production 91, 288–296.

Tanneau, O., Casimir, J. B., Lamary, P., 2006. Optimization of multilayered panels with poroelastic components for an acoustical transmission objective. The Journal of the Acoustical Society of America 120 (3), 1227.

Trabelsi, S., Albouy, P., Rault, J., 2003. Crystallization and melting processes in vulcanized stretched natural rubber. Macromolecules 36 (20), 7624–7639.

Turatsinze, A., Garros, M., 2008. On the modulus of elasticity and strain capacity of Self-Compacting Concrete incorporating rubber aggregates. Resources, Conservation and Recycling 52 (10), 1209–1215.

Williams, P. T., Besler, S., 1995. Pyrolysis-thermogravimetric analysis of tyres and tyre components. Fuel 74 (9), 1277–1283.

Xiao, Y., Wen, J., Wen, X., 2012. Sound transmission loss of metamaterial-based thin plates with multiple subwavelength arrays of attached resonators. Journal of Sound and Vibration 331 (25), 5408–5423.

A Characterization of rubber particles from waste scrap tires

Rubber particles used in this work were kindly supplied by Borcol Tapetes Automotivos situated in Sorocaba, São Paulo State, Brazil. These particles were originated from waste scrap tires. The exact determination of their chemical composition is difficult because tires can be manufactured with different kinds of organic polymers. Styrene-Butadiene Rubber (SBR) is the most commonly used, but natural rubber (polyisoprene), nitrile rubber, chloroprene rubber and polybutadiene rubber can be also used in tires production (Williams and Besler, 1995). This section presents some information related to the chemical characterization of the rubber powder particles used in this work.

Rubber particles used as received are denominated here as not washed. The washed particles were submitted to a washing procedure that consisted in mixing, under occasional agitation, the rubber particles with a saturated $NaOH$ solution during approximately 1 h. The mixture was filtered under vacuum, and the rubber particles were washed with distilled water until the washing water had pH = 7. Rubber particles were dried in a Fanen 515 oven at 100°C until constant mass (drying time was near 6 h).

Washed and not washed rubber particles were sieved in a sieve kit in order to obtain rubber particles with two size ranges. The particles with size from 18 to 35 mesh were denominated M35, and those with size from 35 to 60 mesh are denominated M60. Both (M35 and M60), washed and non washed, were characterized as follows:

1. Fourier Transform Infrared (FTIR) Spectroscopy was carried out in a Cary 630 FTIR - ATR (Attenuated Total Reflectance) from Agilent Technologies equipment, in the range from 4000 cm^{-1} to 400 cm^{-1};
2. Thermogravimetric Analysis (TGA) was carried out in a TGA 2050 thermoanalyzer from TA Instruments, under argon atmosphere, in the range from 25°C to 950°C, with a heating rate of 10°C/min;

3. Differential Scanning Calorimetry (DSC) was carried out in a DSC 200 F3 Maia thermoanalyzer from Netzsch, under argon atmosphere, in the range from -120°C to 250°C, with a heating rate of 10°C/min.

FTIR characterization

Figures A.1, A.2 and A.3 show the FTIR spectra for M35 and M60 samples in two different wave number ranges and for a film of crude styrene-butadiene rubber, respectively. The styrene-butadiene rubber film was obtained by casting a 5% (mass proportion) solution of crude styrene-butadiene rubber (SRB 1502, kindly supplied by Pirelli Pneus situated in São Bernardo do Campo, São Paulo State, Brazil) in chloroform (Synth, P.A. 100%). About 10 g of 5% SBR/$CHCl_3$ solution were placed in a Petri dish (80 mm diameter) and the solvent was allowed to completely evaporate in an exhaustion hood.

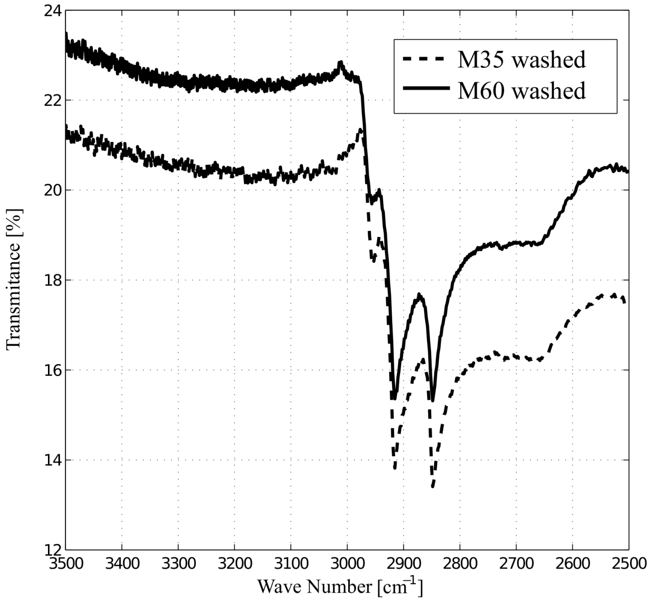

Figure A.1: FTIR spectra for M60 and M35 samples, both washed

In Figures A.1 and A.2, the range from 2500 cm^{-1} to 1800 cm^{-1} was occulted of the FTIR spectra due to the presence of diamond ATR crystal peaks, which cover-up the absorption peaks of rubber particles. In addition, we did not show the spectra of M35 and M60 samples

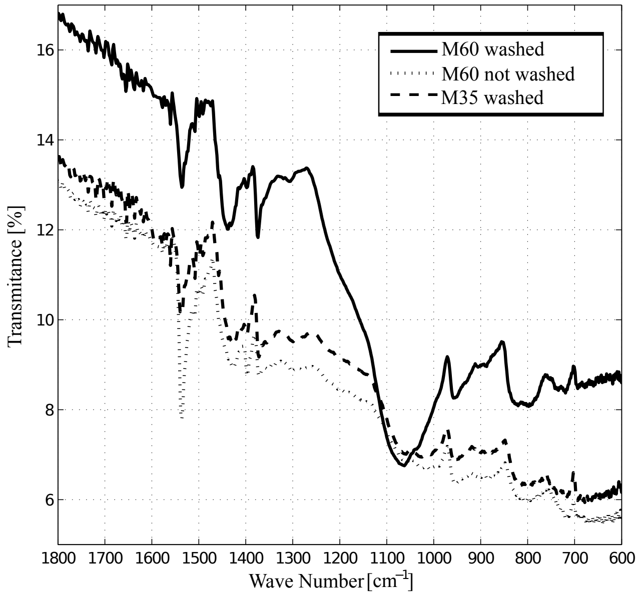

Figure A.2: FTIR spectra for M60 sample (washed and non washed) and for 35M washed

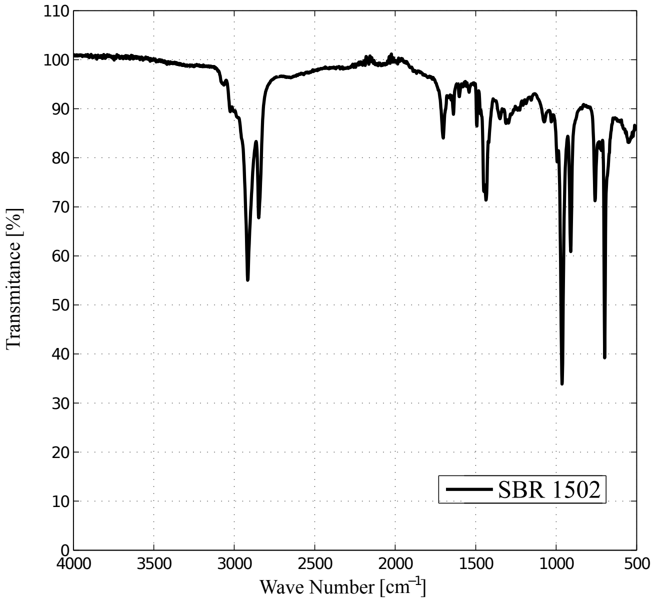

Figure A.3: FTIR spectrum for Styrene-Butadiene rubber

(both not washed) for 4000 cm^{-1} to 2500 cm^{-1} range because they were very similar to those obtained for M35 and M60, both washed. For the 1800 cm^{-1} to 600 cm^{-1} range, the spectrum of M35 washed sample was very similar to that for M35 not washed, and the last one was also occulted.

The main FTIR absorption peaks of rubber particles, which were more clearly observed for M60 (washed) and for crude SBR sample are described in Table A.1. It is also shown the main FTIR absorption peaks for poly (1,4-cis-isoprene) (Galiani, 2010) and for polybutadiene (Nallasamy et al., 2002).

Table A.1: Absorption peaks observed in FTIR spectrum of M60 (washed) and crude SBR

SBR 1502 [cm^{-1}]	M60 washed [cm^{-1}]	Poly (1,4 - cis-isoprene) [cm^{-1}] (Galiani, 2010; Dall'Antonia et al., 2009)	Polybutadiene [cm^{-1}] (Nallasamy et al., 2002; Rocha et al., 2004)
3080			3074
3020	2957 C-H asymmetric stretching (in CH_3 group)	2960	3004 - 2977
2917	2915 C-H symmetric stretching (in CH_3 group)	2920	2918
2848	2848 C-H symmetric stretching (in CH_2 group)	2850	2845
1709			1671
1638			1640 - 1658
1493			
	1536 C=C stretching	1540	
1439	1437 CH_3 asymmetric deformation	1450	1448 - 1436
1340	1374 CH_3 symmetric deformation	1380	1364 - 1344
1312			1308
	1200 (wide) C-H bending and/or CH_2 twist	1250	
1062	1068 (wide) C-CH_2 stretching	1100 - 1020	993
965	954 =C-H in plan deformation		963 (1,4-trans)
907			912
	827 - 820 C-H bending	Region of 800	
759	740 - 720 =C-H out of plane deformation	764 - 741	738 (1,4-cis)
699	694 Styrene group out of plane stretching		700

For M60 washed, it was possible to observe absorption peaks which are only characteristic of poly (1,4-cis-isoprene) (peaks at 1536cm^{-1}, 1200cm^{-1}, and 827-820cm^{-1}), and absorption peaks which are only characteristic only of SBR rubber and polybutadiene (954cm^{-1} and 694cm^{-1}), showing that rubber particles certainly contain poly(1,4-cis-isoprene) and SBR rubber or polybutadiene, or both SBR rubber and polybutadiene.

TGA characterization

Figures A.4 and A.5 show the thermogravimetric analysis with derivative curves for M35 and M60 (washed and not washed), respectively. Table A.2 shows the temperatures of start and finish of the main mass loss (T_1, T_2, T_3 and T_4) and the temperatures of maximum mass loss for the three peaks observed in the derivative curves ($Tmax_1$, $Tmax_2$ and $Tmax_3$). These temperatures were defined according to Figure A.4b. Table A.2 also shows the mass loss percentages occurring at each of the three processes, and the residual char yields at 900°C. Accurate assignment of $Tmax_1$ and T_2 in derivative curves is difficult because first mass loss peak is broad and the second peak seems to start before the first one finishing, however, Figures A.4 and A.5 show that there are clearly three main areas of mass loss.

Table A.2: Temperatures of start and finish of the main mass loss (T_1, T_2, T_3 and T_4) and temperatures of maximum mass loss for the three peaks observed in the derivative curves ($Tmax_1$, $Tmax_2$ and $Tmax_3$) of TGA. mass loss values (in brackets) and residual char yields are also shown. Nomenclature defined in Figure A.4b.

Sample	T_1 [°C]	$Tmax_1$ [°C]	T_2 [°C]	$Tmax_2$ [°C]	T_3 [°C]	$Tmax_3$ [°C]	T_4 [°C]	% of residue at 900°C
M60 washed	155	300	300 (6%)	373	400 (27.6%)	446	490 (25.2%)	37.8
M60 not washed	155	300	300 (6%)	373	400 (27.6%)	446	490 (26.4%)	36.4
M35 washed	159	300	300 (6%)	373	400) (25%)	441	490 (28%)	35
M35 not washed	159	300	300 (6%)	373	416) (26%)	441	490 (26%)	32

Thermal decomposition starts at 155°C to 159°C, and the first mass loss process follows until 300°C for all rubber particles samples, for which the mass loss percentages were 6%. Af-

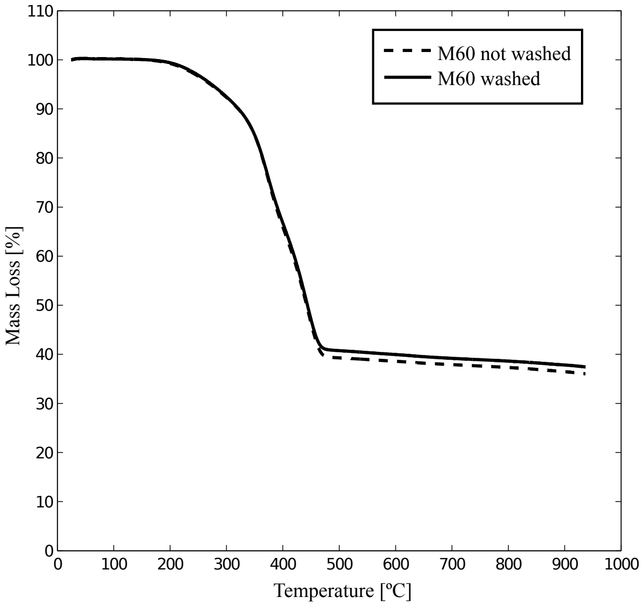

(a) Thermogravimetric analysis for M60 washed and not washed

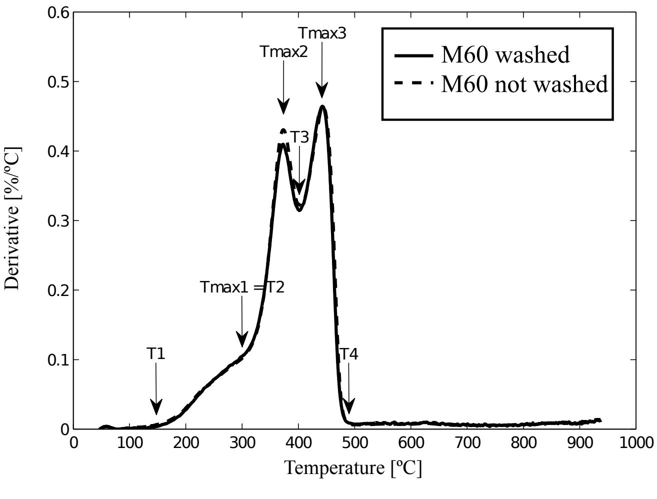

(b) Derivative curves for M60 samples

Figure A.4: Thermogravimetric analysis for M60 samples

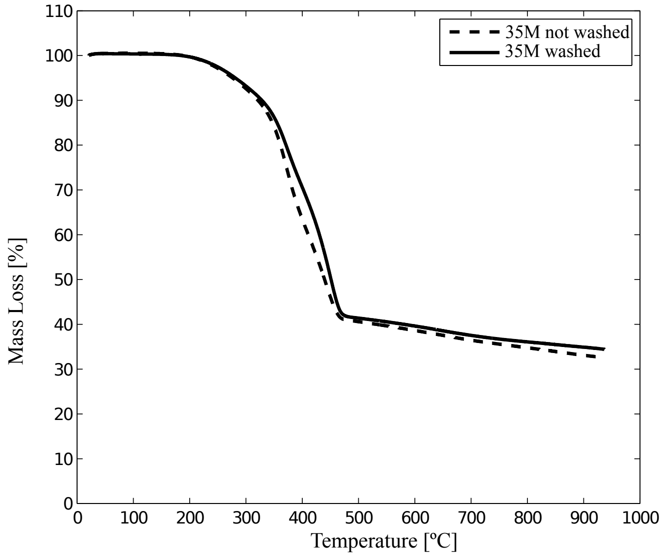

(a) Thermogravimetric analysis for M35 washed and not washed

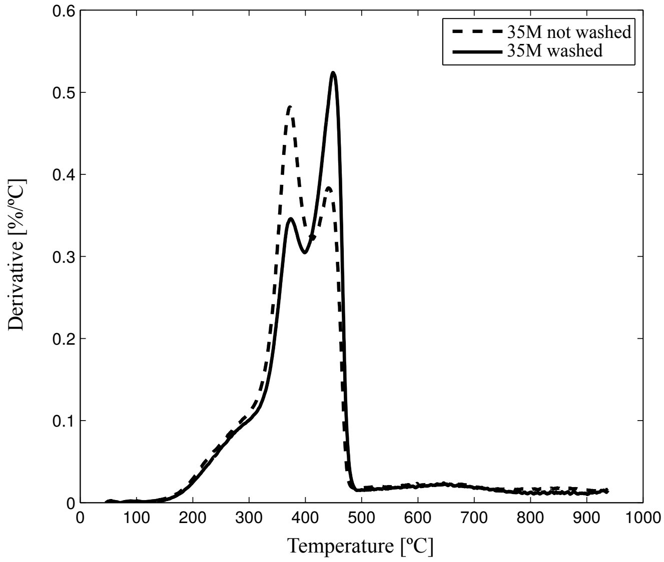

(b) Derivative curves for M35 samples

Figure A.5: Thermogravimetric analysis for M35 samples ter reaching 300°C, the two major mass losses take place, with mass losses of 25% to 28% in each of the two processes. Pyrolysis is essentially complete by 490°C, above which there is no significant mass losses. The residual char yields at 900°C varied from 32% to 37.8%. This behavior was observed for M35 and M60 (washed and not washed) samples, and can be explained by considering the Williams and Besler work (Williams and Besler, 1995). They investigated three different kinds of crushed tires by thermogravimetric analysis, whose rubber chemical composition were (SBR), (tire A), natural rubber (NR) and polybutadiene rubber (BR), (tire B), and SBR, NR and BR (tire C) (Williams and Besler, 1995). There was verified that thermal decomposition started from 240°C to 275°C, depending on tire chemical composition and heating rate used during the pyrolysis process (Williams and Besler, 1995). It was observed two major mass losses (at 375°C and 440°C) for tires B and C, and only one major mass loss for tire A at 440°C (Williams and Besler, 1995). For these samples, the residual char yields were 42%, 32% and 35% for tires A, B, and C, respectively (Williams and Besler, 1995).

Williams and Besler also investigated the thermal behavior of tires “pure” components, and verified that thermal decomposition starts from 325°C (for NR) to 350°C (for SBR or BR), for which the temperatures of maximum mass loss were 375°C for NR and 455°C for SBR (Williams and Besler, 1995). Polybutadiene rubber shows a tendency to two-stage thermal decomposition (with temperatures of maximum mass loss at 400°C and 455°C), but that at 400°C was much less significant (Williams and Besler, 1995). These temperature values were described for a heating rate of 5 $K.min^{-1}$ (Williams and Besler, 1995).

Comparing the results described in (Williams and Besler, 1995) with those shown in Table A.2, we can attribute the first mass loss process observed for M35 and M60 samples to the beginning of natural rubber thermal decomposition added to the thermal decomposition of plasticizing, curatives, and other low molecular mass agents, since tires are a complex mixture of organic and inorganic components. The two following mass loss processes can be associated with NR, and SBR or BR thermal decomposition, respectively. So, it is possible to conclude that M35 and M60 (washed and not washed) certainly contain NR, which is mixed with SBR or polybutadiene rubber (BR), or mixed with both SBR and BR, corroborating with FTIR characterization described above.

DSC characterization

Figures A.6 and A.7 show the Differential Scanning Calorimetry (DSC) curves for M60 and M35 (washed and not washed), respectively, and Table A.3 describes the main thermal transitions. Table A.4 shows glass transition (Tg) and melting temperatures (Tm) for polybutadiene rubber, natural rubber and styrene-butadiene rubber, described in different bibliographic references. For M60 and M35 (washed and not washed) there are a transition near to -60°C, which could be attributed to the NR and SBR glass transitions (Serrano, 2009), but we can not disregard BR, since the glass transition for an amorphous BR with high vinyl content can occur in a large temperature range (from -85°C to 5°C) (Halasa and Massie, 2000).

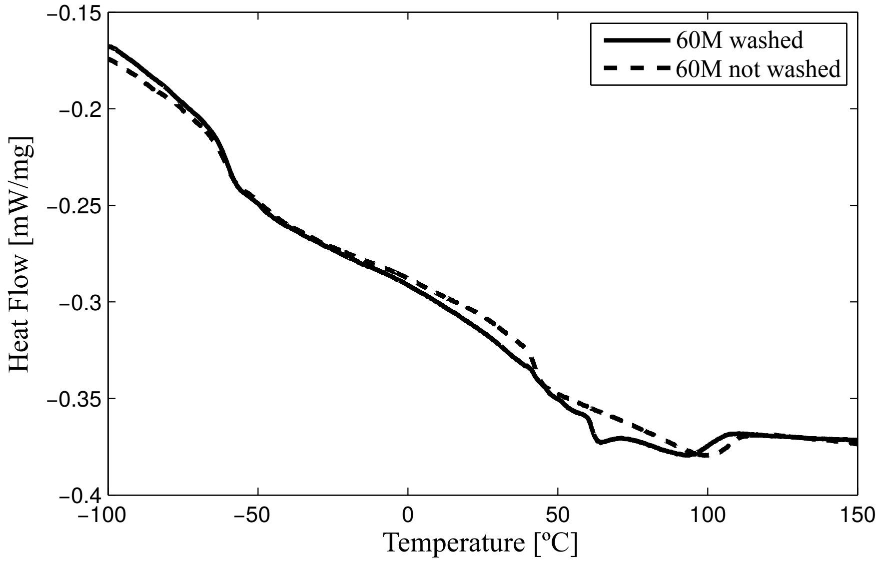

Figure A.6: DSC curve for M60 washed and not washed

DSC curves for M60 and M35 samples show additional thermal transitions above Tg at -60°C. This seems similar to that described in (Halasa and Massie, 2000) for low melting syndiotactic 1,2-polybutadiene. The endothermic peaks at temperature range from 91°C to 99°C can be associated with the melting processes described on Table A.4 for NR and BR (Halasa and

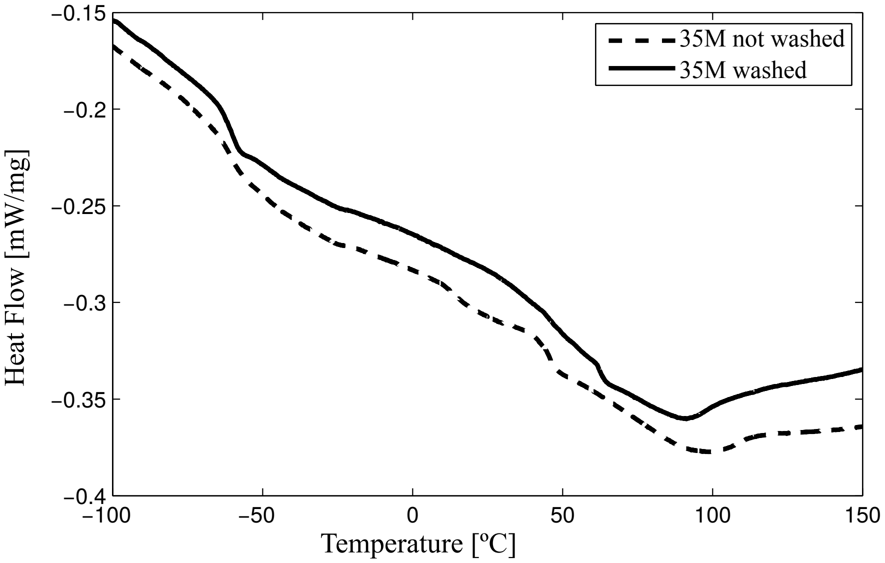

Figure A.7: DSC curve for M35 washed and not washed

Table A.3: Thermal transitions observed in DSC analysis of rubber particles 35M and 60M (washed and not washed)

M35 washed [°C]	M35 not washed [°C]	M60 washed [°C]	M60 not washed [°C]	Transition behavior
-61	-59 (broad)	-60	-61	Baseline change
—	20 (broad)	-50 (weak)	-48 (weak)	Baseline change
63	46	From 40 to 55 (weak) / 63	43	Baseline change / Endothermic peak
91	98	94	99	Endothermic peak

Table A.4: Glass transition (Tg) and melting (Tm) temperatures for polybutadiene rubber (BR), natural rubber (NR) and styrene-butadiene rubber (SBR) reported in literature (Galiani, 2010; Dall'Antonia et al., 2009; Serrano, 2009; Halasa and Massie, 2000; Trabelsi et al., 2003)

Rubber	Thermal transitions (°C)
BR	Tg from -85 to 5 (1,2-polybutadiene, amorphous with high vinyl content) (Halasa and Massie, 2000) Tm from 20 to 60 (1,4-trans and mixtures 1,4-trans/1,4-cis) (Halasa and Massie, 2000) Tm from 150 to 220 (high melting syndiotactic) (Halasa and Massie, 2000) Tg near -10 with Tm from 60 to 105 (low melting syndiotactic) (Halasa and Massie, 2000)
NR	Tg from -66 to -57 (Galiani, 2010; Dall'Antonia et al., 2009); and Tm from 0 to 90 (Trabelsi et al., 2003)
SBR	Tg from -57 to -53 (Serrano, 2009)

Massie, 2000; Trabelsi et al., 2003). In addition, these endothermic peaks can also be related to another process, as described by Serrano (Serrano, 2009), who investigated composites of poly(styrene-co-butadiene) and SBR rubber originated from sole scrap of shoes industry. For these composites, an endothermic peak near to 90°C was also observed and it was associated to residual sulfur (used in almost all rubber cross-linking processes) melting temperature, which is 112.8°C (Serrano, 2009). So, for M35 and M60 samples, this endothermic peak could be also related to the residual sulfur melting.

The thermal transitions observed between Tg (near -60°C) and Tm (near 90°C) for M60 and M35 samples could be explained considering the large Tg range described in literature for polybutadiene rubber, which can present Tg values from -85°C to 5°C (Halasa and Massie, 2000). However, it is interesting also consider a model which have been used to explain the extended glass transition region observed in semicrystalline polymers and filled rubbers (Struik, 1987). This model assumes that crystals disturb the amorphous phase and reduce segmental mobility (for semicrystalline polymers), similar to carbon black particles that restrict the mobility of parts of the rubbery phase (for filled rubbers) (Struik, 1987). The model considers that the polymer chains mobility reduction will be at maximum in the immediate vicinity of the crystals (for semicrystalline polymers) and only at large distances from the crystals will the properties of the amorphous phase become equal to those of the bulk amorphous material (Struik, 1987). The main consequence of this immobilization is that the glass transition will be extended towards the high-temperature side (Struik, 1987). Above Tg of the bulk amorphous material, some parts of the amorphous phase are rubbery, other parts are glassy, and still other parts will just be passing through their glass transitions (Struik, 1987). Therefore, in a semicrystalline polymer, the amorphous phase will not have a single Tg, but a Tg-distribution (Struik, 1987). The lowest glass transition temperature will be equal to the Tg of the bulk amorphous material (or higher, when the amorphous phase is totally disturbed), and the highest Tg, named TgU, will depend on the interactions between the crystalline and amorphous phases (Struik, 1987).

For filled rubbers, Struik (Struik, 1987) observed that, if the adhesion between filler and rubber is sufficiently strong, there is a “glassy shell” around the filler particles in which the polymer chains are immobilized, and will remain intact, unless higher temperatures are reached. When temperature increases, this glassy shell will decrease in thickness and the polymer chains present in this region will enter the glass transition (Struik, 1987). As a consequence, at temperatures above Tg, filled rubbers may show the same extended/broad glass transition effects as semicrystalline polymers (Struik, 1987). This could also explain the presence of others thermal transitions above Tg (-60°C) visualized for M35 and M60 samples.

It is also interesting to note that the thermal transitions above Tg (-60°C) seems to be affected by the washing procedure of M35 and M60 rubber particles. Transitions that occur from 40°C to 63°C (third line on Table A.3) seems to be more affected than the others. For M35 and M60, both not washed, the transition occurred near 40°C (for M35 at 46°C and for M60 at 43°C) changed to higher temperatures (to 63°C for M35 and M60, it started at 40°C and finished at 63°C). This behavior could be attributed to two main effects: plasticizing (and other low molecular mass organic components) removal by the washing process, and/or thermal history effects, since samples were dried at 100°C during approximately 6 h after washing. As the TGA results did not show mass losses until 155°C to 159°C, this behavior could be associated to thermal history effects.

B MATLAB algorithms

MATLAB Script file to calculate TL is presented in the following:

```matlab
% Transmission loss calculation for impedance tube measurement using the Transfer Matrix Method
% For BSWA SW433 impedance tube measurements, d12 = 45e-3 and e d34=45e-3.

clear all; close all; clc

filename = 'FRF_file.mat'; % file name with the measured FRFs
autopower = 'PSD_file.mat'; % file name with measured PSD

%% data entered by the user

d = 25e-3;          % Sample thickness [m]
T = 24;             % Air temperature [oC]
P0 = 94100;         % Atmospheric pressure [Pa]

x2 = -35e-3;        % Distance from mic 2 to sample surface [m]
x3 = 100e-3;        % Distance from mic 3 to sample surface [m]
d12 = -45e-3;       % Distance between mic 1 and mic 2 [m]
d34 = 45e-3;        % Distance between mic 3 and mic 4 [m]

gamma = 1.4;        % specific heat ratio [dimensionless]
R = 287.058;        % ideal gas constant for dry air [J/kg/K]

%% Data processing
% Distance from mic 1 and mic 4 calculation
x1 = x2+d12;
x4 = x3+d34;

% Air properties calculation
rho0 = P0 ./ (R * (T + 273.15));          % Density [kg/m^3]
c = sqrt(gamma .* R .* (T + 273.15));     % Speed of sound [m/s]

% Reading of .mat file obtained from the LMS
load(['./' filename])

df = FRF.x_values.increment;     % Measurement resolution [Hz]
N = FRF.x_values.number_of_values; % Number of taken values
f = 0:df:(N*df)-df;      % Frequency vector [Hz]
w = 2*pi*f;         % Angular frequency vector [rad/s]
k = w./c;           % Wave number [m^-1]

% PSD reference signal from the loudspeaker
load(['./' autopower])

PSD = PSD.y_values.values'; % Power Spectral Density from the LMS [V^2/Hz]
Grr = PSD.*df;  % Auto-spectrum [V^2]

% Obtained FRF between Pi and the reference signal Pr
Hr1 = FRF.y_values.values(:,1).';
Hr2 = FRF.y_values.values(:,2).';
Hr3 = FRF.y_values.values(:,3).';
```

```
Hr4 = FRF.y_values.values(:,4).';

% A, B, C and D coefficients calculation
A = sqrt(Grr(1,:)).*1j.*((Hr1.*exp(1j*k.*x2)-Hr2.*exp(1j*k.*x1))./...
        (2*sin(k.*(x1-x2))));
B = sqrt(Grr(2,:)).*1j.*((Hr2.*exp(-(1j*k.*x1))-Hr1.*exp(-(1j*k.*x2)))./...
        (2*sin(k.*(x1-x2))));
C = sqrt(Grr(3,:)).*1j.*((Hr3.*exp(1j*k.*x4)-Hr4.*exp(1j*k.*x3))./...
        (2*sin(k.*(x3-x4))));
D = sqrt(Grr(4,:)).*1j.*((Hr4.*exp(-1j*k.*x3)-Hr3.*exp(-1j*k.*x4))./...
        (2*sin(k.*(x3-x4))));

% Pressure and particle velocity in x=0 and x=d
p_x0 = A+B;
v_x0 = (A-B)./(rho0*c);
p_xd = C.*exp(-1j*k*d)+D.*exp(1j*k*d);
v_xd = (C.*exp(-1j*k*d)-D.*exp(1j*k*d))./(rho0*c);

% T matrix components calculation assuming a reciprocal nature of the
    samples
den = p_x0.*v_xd+p_xd.*v_x0;
T11 = (p_xd.*v_xd+p_x0.*v_x0)./den;
T12 = (p_x0.^2-p_xd.^2)./den;
T21 = (v_x0.^2-v_xd.^2)./den;
T22 = T11;

% For anechoic termination measurements, Reflection and Transmission
    coefficients:
Ra = (T11+(T12./(rho0*c))-T21.*rho0*c-T22)./...
      (T11+(T12./(rho0*c))+T21.*rho0*c+T22);
Ta = (2*exp(1j*k.*d))./(T11+(T12./(rho0*c))+T21.*rho0*c+T22);
Za = (T11+T12./(rho0*c))./(T21+T22./(rho0*c)); % Normal impedance

% Transmission Loss obtaining
TL = -20*log10(abs(Ta));
TL_filtrado = smooth(TL,50);

%% Plots
semilogx(f,TL_filtrado,'LineWidth', 2),
xlabel('Frequency [Hz]'), ylabel('TL [dB]')
grid on
```

An adaptation to TL script is made in order to calculate the absorption coefficient and following lines must be added:

```
% Name of the data obtained on the tube
filenameAlpha = 'FRFs_alpha.mat';
N=10;

% Experimental FRFs
FRF_mic_1 = FRF.y_values.values(:,1).';
FRF_mic_2 = FRF.y_values.values(:,2).';

% H21 obtantion
H21 = FRF_mic_2 ./ FRF_mic_1;

% Complex reflection coefficient
alpha_r = (exp(2*1i.*k.*(1 + d12))).* (H21 - exp(-1i.* k.* d12))./(exp(1i.*
    k.*d12) - H21);

% Pre processing, forces the real and imaginary parts at the begining of
    the vector
alpha_r_real = real(alpha_r);
alpha_r_imag = imag(alpha_r);
alpha_r_real(1 : N) = 1;
alpha_r_imag(1 : N) = 0;
alpha_r_real_smooth = smooth(alpha_r_real,10);
alpha_r_imag_smooth = smooth(alpha_r_imag,10);
alpha_r_ajustado = (alpha_r_real_smooth + 1i * alpha_r_imag_smooth).';

% Absorption coefficient
alpha_ajustado = 1 - (abs(alpha_r_ajustado)).^2;
c_absorcao = smooth(alpha_ajustado);

%% Plots
plot(f, c_absorcao([1,3],:), 'LineWidth', 2), grid on, hold on
xlabel('Freq. [Hz]'), ylabel('\alpha')
```